



INAOE

# **Automated Method to Assist Breast Cancer Diagnosis**

by

**Jonathan Hernández Capistrán**

Dissertation  
Submitted to the Department of Electronics  
In Partial Fulfillment of the Requirements for the Degree of  
Doctor of Science

**Doctor of Science in Electronics**

at the

National Institute for Astrophysics, Optics and Electronics  
December 2019  
Tonantzintla, Puebla, México

Supervised by

**Jorge Francisco Martínez Carballido, Ph. D.**

©INAOE 2019  
All rights reserved

The author hereby grants to INAOE permission to reproduce  
and to distribute copies of this thesis document in whole or in part



## Abstract

---

Breast cancer is the top cause of deaths by cancer in women worldwide. Methods for early detection of breast cancer are of great help to improve prognosis of patients, providing less aggressive treatment, and better time/cost performance. Stage 0 of cancer, also known as pre-cancer, is not palpable and is only detected by screening mammogram examination. Therefore, the detection of cancer in this stage is desirable. This stage is characterized by lesions, known as *micro-calcifications* (MCs), the first clinically observable lesions, indicating such disease. Their typical size is less or equal to 1 mm, that is why it is difficult to be detected by an expert. In recent years, different methods, for *micro-calcification detection* on *mammograms* (X-ray images from the breast), have been proposed; however, the issue is still open to reach acceptable levels of *detection rate* and *false alarm rate*, preventing its use as a pre-diagnostic tool.

This work analyzes and proposes a new and simple system for *detection of MCs*, based on the use of the two most used public mammogram data sets, MIAS and DDSM. We first, analyze how an expert detects MCs in an image and which are its distinctive characteristics; such as intensity values of the surrounding tissue and the prominent peak in a MC. Therefore, a classification according to their local surroundings: obvious, subtle and clusters. Additionally, a new MC detection method based on (1) morphologic segmentation for detection of *regions of interest* (ROIs), (2) extraction of few and effective attributes from candidates to MCs, and (3) one classification stage with two different classifiers, *k Nearest Neighbor* (kNN) and *Support Vector Machine* (SVM). For dense mammograms in MIAS database with a *sensitivity* of 0.9752, *false alarm rate* of 0, *accuracy* of 0.9876, and 0.9951 for *area under the ROC curve* using SVM, for a classifier. The proposed MC detection method achieves *sensitivity*, *false positive rate*, *accuracy* and *area under the ROC curve* of 0.9664, 0.0224, 0.9683 and 0.9934 for the MIAS data set; and 0.9386, 0.0526, 0.9664 and 0.9742 for the DDSM data set. The proposed method gives better results than those from state-of-the-art

literature, when the mammograms are classified in *fatty*, *fatty-glandular*, and *dense*. Methods, that report results for dense mammograms, have poor performance; however, the presented method shows the best performance for dense mammograms.

## *Resumen*

---

El cáncer de mama es la principal causa de muerte por cáncer en mujeres de todo el mundo. Los métodos para la detección temprana del cáncer de seno son de gran ayuda para mejorar el pronóstico de las pacientes, ya que proporcionan un tratamiento menos agresivo y un mejor desempeño en tiempo- costo. La etapa 0 del cáncer, también conocida como pre-cáncer, no es palpable y solo se detecta mediante un examen de mamografía. Por lo tanto, la detección de cáncer en esta etapa es deseable. Esta etapa se caracteriza por lesiones, conocidas como microcalcificaciones (MC), las primeras lesiones clínicamente observables, que indican dicha enfermedad. Su tamaño típico es menor o igual a 1 mm, por eso es difícil que un experto lo detecte. En los últimos años, se han propuesto diferentes métodos para la detección de microcalcificaciones en mamografías (imágenes de rayos X del seno); sin embargo, el problema aún está abierto para alcanzar niveles aceptables de tasa de detección y tasa de falsos positivos, evitando su uso como herramienta de diagnóstico previo. Este trabajo analiza y propone un sistema nuevo y sencillo para la detección de MC, basado en el uso de los dos conjuntos de datos de mamografías públicas más utilizados, MIAS y DDSM. Primero, analizamos cómo un experto detecta los MC en una imagen y cuáles son sus características distintivas; tales como los valores de intensidad del tejido circundante y el pico prominente en un MC. Por lo tanto, una clasificación de acuerdo con su entorno local: obvio, sutil y agrupaciones. Además, un nuevo método de detección de MC basado en (1) segmentación morfológica para la detección de regiones de interés (ROI), (2) extracción de relevantes características de candidatos a MC, y (3) una etapa de clasificación con dos clasificadores kNN y SVM. Para mamografías densas en la base de datos MIAS con una sensibilidad de 0.9752, tasa de falsa alarma de 0, precisión de 0.9876 y 0.9951 para el área bajo la curva ROC usando SVM, como clasificador. El método de detección de MC propuesto logra sensibilidad, tasa de falsos positivos, precisión y área bajo la curva ROC de 0.9664, 0.0224, 0.9683 y 0.9934 para el conjunto de datos MIAS; y 0.9386, 0.0526, 0.9664 y 0.9742 para el conjunto de datos DDSM. El método propuesto ofrece mejores resultados que los de la literatura actual, cuando las mamografías

se clasifican en grasosas, glandulares grasosas y densas. Los métodos, que informan resultados de mamografías densas, tienen bajo rendimiento; sin embargo, el método presentado muestra el mejor rendimiento para mamografías densas.

## ***Agradecimientos***

---

Agradezco a Dios en primer lugar por ayudarme en todo y nunca fallarme. “*Jehová es mi fortaleza y mi cántico, Y ha sido mi salvación. Este es mi Dios, y lo alabaré; Dios de mi padre, y lo enalteceré.*” Éxodo 15:2

Agradezco a mi esposa, por apoyarme en esta hermosa etapa de mi vida y superar las dificultades junto a nuestro Dios.

Agradezco a mis padres por haberme enseñado todo, tanto científico, emocional y espiritual para cumplir esta meta.

Agradezco a mi hermano por ayudarme y darme ánimos para seguir adelante.

Un agradecimiento especial a mi director de tesis Jorge Martínez Carballido por ser mi mentor, guía y consejero.

Agradezco también al CONACYT por la beca doctoral con cvu 414681.

Esta investigación fue realizada gracias al apoyo parcial del Consejo de Ciencia y Tecnología del Estado de Puebla.

## *Dedicatoria*

---

*“Y a todo lo creado que está en el cielo,  
y sobre la tierra, y debajo de la tierra,  
y en el mar, y a todas las cosas que  
en ellos hay, oí decir: Al que está  
sentado en el trono, y al Cordero,  
sea la alabanza, la honra, la gloria y  
el poder, por los siglos de los siglos.”*

*Apocalipsis 5:13*



# ***Contents***

---

<b>Abstract</b>	<b>i</b>
<b>Resumen</b>	<b>iii</b>
<b>Agradecimientos</b>	<b>v</b>
<b>Dedicatoria</b>	<b>vii</b>
<b>Contents</b>	<b>viii</b>
<b>List of Figure</b>	<b>x</b>
<b>List of Tables</b>	<b>xii</b>
<b>Introduction</b>	<b>1</b>
1.1 Background	1
1.2 State of Art	5
1.3 k Nearest Neighbor (kNN) classifier	10
1.4 Support Vector Machine (SVM) classifier	10
1.5 Summary	10
<b>Methods</b>	<b>12</b>
2.1 Problem Statement	12
2.2 Dissertation Goals	17
2.2.1 General Goal	17
2.2.2 Specific Goals	17
2.2.3 Dissertation Contribution and Organization	17
2.3 Material and Methods	17
2.3.1 Mammogram data sets	17
2.4 Microcalcification Segmentation	23

2.5	Microcalcification modelling and classification.....	28
2.6	Extraction of micro-calcifications candidates from abnormality clusters	29
2.7	Summary .....	39
<b>Results</b>	.....	<b>40</b>
3.1	Microcalcification segmentation results .....	40
3.2	Microcalcification model for detection.....	40
<b>Conclusion and future work</b>	.....	<b>48</b>
4.1	Discussion .....	48
4.2	Conclusion .....	49
4.3	Future Work .....	51
4.4	Contributions .....	51
<b>References</b>	.....	<b>53</b>
<b>Appendix A</b>	.....	<b>66</b>
<b>Appendix B</b>	.....	<b>67</b>

## *List of Figure*

---

Figure 1. Common process in a mammography test, and delivery time per test type. .	1
Figure 2. a) Craniocaudal and b) mediolateral oblique views. Under each view is shown how the images are taken [8].	2
Figure 3. Breast Cancer Staging measures the spread of the disease upon diagnosis. [15]	4
Figure 4. Most common breast cancer types.[18]	5
Figure 5. Principal areas of breast cancer research. At the right of the figure shows the process that a specialized medic performs (Screening and Diagnosis).	6
Figure 6. The two most common breast cancer screening programme.	14
Figure 7. Human error in the analysis of a mammogram	15
Figure 8. Proposed and actual screening process.	16
Figure 9. Principal regions from a mammography	20
Figure 10. General pre-process for breast extraction	21
Figure 11. Digital mammogram, from the MIAS data set, with one cluster of micro-calcifications.	22
Figure 12.- Breast density variety [74]	24
Figure 13. Classification of MCs according to their surrounding tissues; a) Subtle, b) obvious and c) Cluster type.	24
Figure 14. Examples for some Weber contrast values of a) subtle b) normal and c) obvious groups.	26
Figure 15. General process in the Microcalcifications segmentation	27
Figure 16. Different stages for detection of micro-calcifications, segmentation, binarization, feature extraction, and classification.	29
Figure 17. Three-dimensional visualization of one micro-calcification on a digital mammogram.	35

Figure 18. Region of interest (left part) along with the corresponding mask of three surface levels (right part). Overlapping the ROI and the mask allows the extraction of information from different surface levels for sub-sequent feature extraction.....	36
Figure 19. General process to detect and classify a MC .....	38
Figure 20. ROC (TPR vs. FPR) obtained by testing the method with the SVM classifier on three different data sets, MIAS (red curve), DDSM (blue curve), and the combination of both data sets (orange curve). ....	43
Figure 21. ROC (TPR vs. FPR) obtained by testing the method with the kNN classifier on three different data sets, MIAS (red curve), DDSM (blue curve), and the combination of both data sets (orange curve). ....	43
Figure 22. ROC (TPR vs. FPR) obtained by testing the method with the SVM classifier on the MIAS data set for each density group, fatty (purple curve), fatty-glandular (blue curve), and dense (green curve). ....	44
Figure 23. ROC (TPR vs. FPR) obtained by testing the method with the kNN classifier on the MIAS data set for each density group, fatty (red curve), fatty-glandular (green curve), and dense (black curve). ....	44

## *List of Tables*

---

Table 1. Relevant papers and their principal characteristics .....	9
Table 2. Number of radiologist and mammography units in five different countries. 12	
Table 3. Description of MIAS data set in terms of breast density. ....	18
Table 4. Description of DDSM data set in terms of abnormality. ....	19
Table 5. General algorithm for extraction of ROIs from ground truth images. ....	23
Table 6. Range of values for weber contrast measures of different groups .....	25
Table 7. Random generation of a set of n micro-calcification candidates from the set of normal images without abnormality clusters identified by the radiologist.....	29
Table 8. State of the art Comparison diversity.....	34
Table 9. Total result accordance to category and techniques.....	40
Table 10. Performance of different methods for detection of micro-calcifications....	45
Table 11. Comparison with our proposed method and the two-best result in literature .....	49

# Introduction

---

## 1.1 Background

In 2018, there was 2,093,876 (11.6 % of the total of global new cancer cases) of new cases of breast cancer, causing 1,761,007 number of deaths [1].

Numerous experiments have established that an early detection of breast cancer eases the treatment, reducing risks, as well as the mortality percentage in 25% [2]. For early detection, *mammography* is an imaging tool with high sensitivity and it is the most recommended by the guidelines of the World Health Organization [3] [4].

There are two principal tests performed by a specialized radiologist, screening and diagnostic mammograms [5]. Screening mammogram is used in women who have no symptoms; this has the purpose to be widespread for early diagnosis; meanwhile diagnostic mammograms is used when some breast lesion or a change is seen on a screening mammogram. In USA, a mammogram take per breast is completed in 15 minutes [6]; a screening type exam takes from one to two hours interpreting the mammogram by a technician and 5 to 7 days to get the final results by radiologist [7], Figure 1. This delivery time is mainly because radiologists specialized in the analysis of mammography are fewer compared with the number of mammograms to analyze.

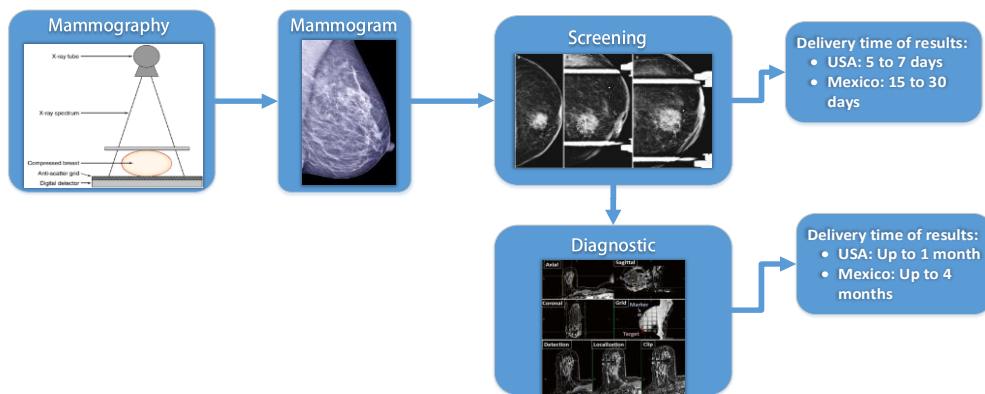
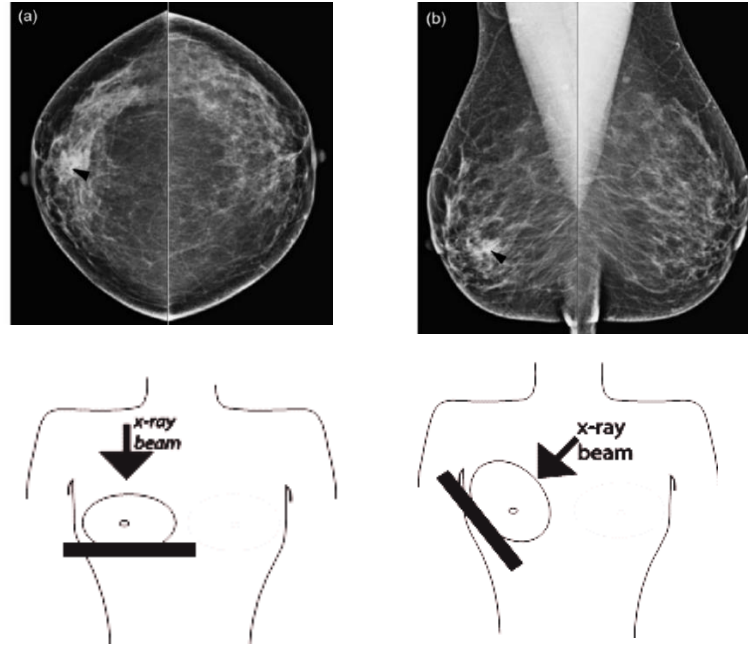


Figure 1. Common process in a mammography test, and delivery time per test type.

Standard views are performed on screening mammograms and it consist of 4 views. The two views for each breast are shown in Figure 2: (a) craniocaudal and (b) mediolateral oblique; these projections are not orthogonal [8]. For screening purposes, the mediolateral oblique is used. Craniocaudal views are used to confirm when in doubt on some lesions detected for the screening process.



*Figure 2. a) Craniocaudal and b) mediolateral oblique views. Under each view is shown how the images are taken [8].*

At the late 1980's with the introduction of magnification views [9] the detection of microcalcification was possible even when the invention of mammography was in the late 1950s. It was until 1992 that the Breast Imaging Reporting and Data System was created. Therefore, the detection of microcalcification in a mammogram is a relatively new area.

The public database most used is mini-MIAS [10], it was published on 1994 and by popular request, the original MIAS Database (digitized at 50 micron pixel edge) was reduced to 200 micron pixel edge and clipped/padded so that every image is  $1024 \times 1024$  pixels. The second most used database is DDSM [11] was published in 2001 using scanners with different resolution between 42 micron to 50 microns. Both of this database are digitized, this type of database is known as Screen Film Mammography

(SFM). In 2000 the Food and Drug Administration approved the first digital mammography (DM) known as full-field digital mammography. DM images are mostly used combined with computer-aided detection (CAD); which is a method that analyzes the mammographic images for suspicious areas and considered a second reader. The American College of Radiology (ACR) says that CAD systems, when used for screening, can be a valuable procedure in the early detection of breast cancer [12]. The major difference between these two types of database is that SFM are images that are acquired on x-ray film, and then digitized. Whereas, DM is a mammography system in which the X-ray film is replaced by solid-state detectors that convert X-rays into electrical signals, improving resolution and contrast making it easier to view small lesions on high density breast. An example of this type of database is the INbreast [13] with a solid-state detector of amorphous selenium, pixel size of 70 (microns), and 14-bit contrast resolution.

To diagnose how far the cancer has been spread there is a process called staging. The stage of a cancer describes how much cancer is in the body. It also helps to determine how aggressive the cancer is and how to treat it. Cancer stages are often used as a survival statistic. Stage-0, also known as pre-cancer, it means that not spread beyond where it started to other parts of the breast or other organs. This stage does not usually cause symptoms and is not palpable. Usually, it is discovered while carrying out an imaging test as mammograms. As well, it is the earliest stage of breast cancer. Stage zero (stage 0) breast cancer is also known as carcinoma in situ. According to the American Cancer Society, people with a type of breast cancer that has not spread beyond the breast tissue have a 5-year survival rate of 99%. This survival rate means that 99% of women with stage 0 breast cancer live at least 5 years after diagnosis. [14], as is shown in Figure 3.



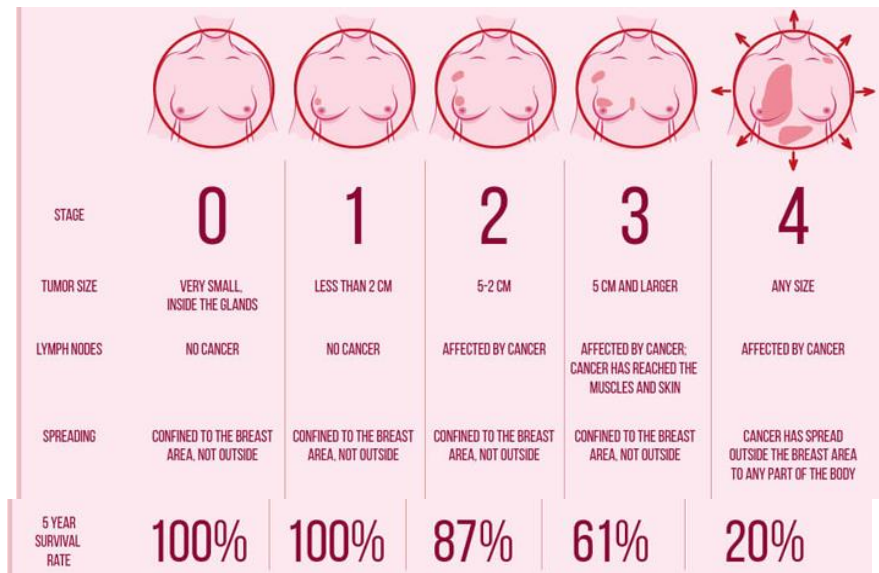


Figure 3. Breast Cancer Staging measures the spread of the disease upon diagnosis. [15]

Breast cancer originates in the epithelial cells that lie at the lobules and ducts; and under normal conditions these epithelial cells are responsible for making milk [16]. When there is a malignant change in these cells, *carcinoma* or *cancer* happens. The types of breast cancer are defined based on the type of tissue and on where the cancer begins. *Invasive Ductal Carcinoma* (IDC) is the most common type of breast cancer detected where *invasive* means that the cancer has spread to the surrounding breast tissues and *ductal* means that the carcinoma began in the ducts. IDC. Is the most common cancer detected because most women get a mammogram at a late stage. At Stage-0 the cancer cells are confined to a very limited area. This stage includes noninvasive breast cancer lobular carcinoma in situ (LCIS) and ductal carcinoma in situ (DCIS), this is usually found by mammography, as old cancer cells die, tiny specks of calcium, called *micro-calcifications* (MC), form within the broken-down cells. The mammogram shows the cancer cells inside the ducts as individual or cluster of these micro-calcifications (MCs), which appear either as white specks or as a shadow [17]. Even though Stage-0 breast cancer is considered “non-invasive,” it does require immediate treatment, typically surgery or radiation, or a combination of both. Chemotherapy is usually not part of the treatment regimen for earlier stages of cancer. The most common types of breast cancer and, the percentages of appearance are shown in the Figure 4.

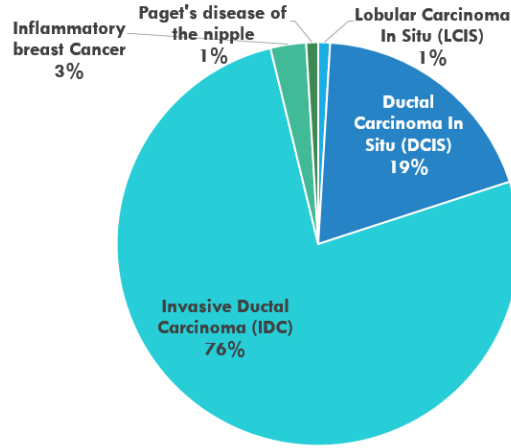


Figure 4. Most common breast cancer types.[18]

Breast microcalcification are lesions whose diameter is inferior to 1 mm. Also, malignant MCs are typically less than 0.5 mm and, according to [19], mammographs with resolution of 50  $\mu\text{m}$  or better can be used to detect MCs, without magnification, of size around 500  $\mu\text{m}$ .

## 1.2 State of Art

In what follows a review of state of the art in relevant and related work to this proposal.

Research about breast cancer based on mammography images has three stages; *pre-processing*, *segmenting* and *classifying*. These areas are shown in Figure 5. In the pre-processing stage, has four areas; breast segmentation, pectoral segmentation, density analysis and mammogram enhancement. The objective in breast and pectoral segmentation is to eliminate, from SFM images, any object or artifact that is no part of the breast such as labels, markers, scratches and even adhesive tape [20]. State of the art research has proposed many algorithms such as: as Margin Setting Algorithm (MSA) [21], active contours [22], fuzzy logic [23], [24], thresholding algorithms [25]. texture analysis [26], morphological operations [27], line detection [28], [29], wavelet transform [30], global an local threshold [31], [32].

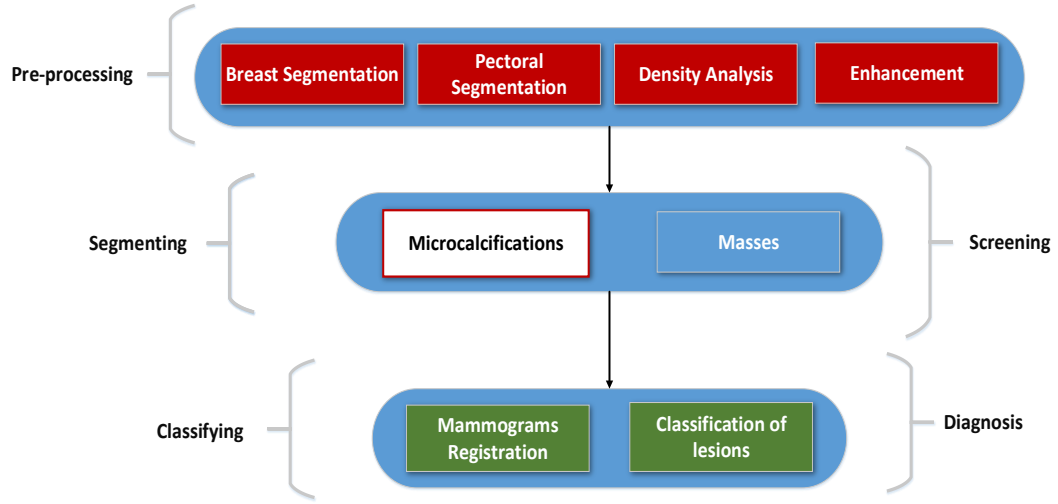


Figure 5. Principal areas of breast cancer research. At the right of the figure shows the process that a specialized medic performs (Screening and Diagnosis).

For segmentation stage, there are two types of detections: microcalcifications and masses. Several algorithms to detect these lesions have been using methods such as: multilevel thresholding [33], deep learning [34], fuzzy logic [35], texture analysis [35], cellular neural network [36], [37], wavelet [38] Gabor [37] feature extraction [39] and others. However, in several reported research work, start with sub-images of the mammogram and then use them to detect the lesions for the given region of the full image. It is not clear, but one could assume that the sub-images are manually segmented and with a specified method.

Published work uses publicly available data sets along with ground truth (GT) to test their proposed methods for comparison purposes as MIAS and DDSM. Some researchers have used private data sets [40] [41], provided by a collaborating hospital.

In 2014, one method is proposed [42] where *segmentation* is obtained by using a LoG filter, followed by a *clustering method*, based on Fuzzy C-means with Features (FCM-WF). It was tested on simulated clusters of micro-calcifications, implying that the location of the cluster, within the breast, and the exact number of micro-calcifications are known. This method uses the MIAS and a private data set. The method is tested in 20 images where all of them contain micro-calcifications. In the same year, a second method is presented [43]. It is divided in a three-step process beginning with

*enhancement* by Histogram equalization (HE) and Morphological Enhancement, followed by *segmentation*, based on Otsu's threshold, of the region of interest for identification of micro calcifications and mass lesions, and the last stage *classifies* between normal and micro-calcifications and then it discriminates between benign and malignant micro calcifications. In the *classification stage*, three methods were used, the voting K-Nearest Neighbor classifier (K-NN), Support Vector Machine classifier (SVM) and Artificial Neural Network classifier (ANN). The method is tested with 181 images out of 322 images from the MIAS data set. A third method was proposed in the same year [44]. It divided into two main sections, detection of potential MCs region (PMR) and PMR classification to true and false positive regions using wavelet decomposition transform. Experiments were performed on 50 out of 322 MIAS images and 140 DDSM images.

In 2015, one proposed method [45] consists of three stages, where (1) pre-processing is applied for ROI detection and image improvement using Non-Subsampled Contourlet Transform (NSCT) and Super Resolution (SR); (2) several image features are extracted, and skewness of each feature is calculated; and (3) an *AdaBoost* algorithm is used for classification and to determine the probability of benign and malign disease. This method uses 288 out of 322 MIAS images. In the same year, there is a method [46], where the topology/connectivity of individual micro-calcifications is analyzed within a cluster using multiscale morphology; a set of micro-calcification graphs is generated to represent the topological structure of micro-calcification clusters at different scales; and graph theoretical features are extracted, which constitute the topological feature space for modeling and classifying micro-calcification clusters. The k nearest neighbor classifier is employed for classifying micro-calcification clusters. The method works with 20 micro-calcifications from the MIAS data set where 9 are classified as malignant and 11 as benign. It also works with 25 micro-calcifications from the DDSM data sets with 14 of them classified as malignant and 11 as benign. A third method is proposed in 2015 [47], where the micro-calcification segmentation method is based on

the geodesic active contours (GAC) technique associated with anisotropic texture filtering. This method employs 158 out of 540 DDSM images.

In 2016, a proposed method [41] removes label and pectoral muscle adopting the largest connected region marking and region growing method; then, it enhances MCs using a combination of double top-hat transform and grayscale-adjustment function; then, it removes noise and other interference information and retains significant information by modifying the contourlet coefficients using nonlinear function; finally, it uses a non-linking simplified pulse-coupled neural network to detect MCs. The method analyzes 23 MIAS digital mammograms containing MCs (7 glandular, 10 dense, and 6 fatty) and 50 mammograms without MCs (15 Glandular, 20 Dense, 15 Fatty). A second method [48] uses the location of micro-calcifications as well as topological information (connectivity) of these micro-calcifications and individual approaches (location or topology). For the topology aspects, there is extraction of regions of interest which contain micro-calcification clusters. Subsequently, morphology is used to grow detected micro-calcification and extract their connectivity over a number of scales, which generates a topology feature vector. Classification is based on a k nearest neighbor classifier. For location aspects, full mammograms and the cluster locations are used to generate probabilistic maps where the feature space contains relative locations within these maps, which are fed into an appropriate learning machine. As a final step, features from both, topology and location information, are combined to form an overall feature vector which can be used as the basis for classification. This method is applied to 20  $512 \times 512$ -pixel ROIs from MIAS data set and to 134 malignant MCs and 146 benign MCs from the DDSM data set.

In one paper [48], from 2017, a hidden Markov tree model of dual-tree complex wavelet transform is applied for micro-calcification diagnosis. The correlation between different wavelet coefficient is captured. The system is applied to 26 MIAS ROIs with 12 benign and 14 malignant and to 150 DDSM ROIs with 82 of them benign and 68 malignant. In a second approach [49], from 2017, structured microcalcifications on an abnormal mammogram are detected, based on multiscale products of eigenvalues of

the Hessian matrix. The detected image contains calcifications along with background information. To eliminate the unnecessary background information, the response image, coming out from Hessian matrix approach, is passed to a thresholding technique such as a probability density function based Tsallis entropy, in which potential micro-calcifications are segmented efficiently. The method is applied to 234 clusters (150 normal and 84 abnormal), extracted from MIAS, USCF; and to clusters from the DDSM data set, with 27 abnormal and 18 normal. In Table 1 presents information from relevant papers. This table presents the database, number of images they use and which is the main pupose of the paper. Chaper 3 uses this table for comparision with the results of our proposed work.

*Table 1. Relevant papers and their principal characteristics*

	<b>Database</b>	<b>Images</b>	<b>Purpose</b>
[50]	DDSM	158 out of 540	MC's segmentation
[45]	<i>MIAS</i>	<i>288 out of 322</i>	<i>Masses and MC's Segmented and classify</i>
[43]	MIAS	181 out of 322	MC's segmentation
[42]	<i>MIAS and private</i>	<i>20 out of 20 only MC's images</i>	<i>MC's segmentation</i>
[44]	DDSM, MIAS	50 out of 322 MIAS - 140 DDSM	MC's segmentation
[25]	MIAS and private		MC's segmentation
[51]	MIAS DDSM Combined	50 out of 322 MIAS - 197 DDSM	MC's classification
[52]	MIAS		MC's classification

### 1.3 k Nearest Neighbor (kNN) classifier

The *k nearest neighbor* (kNN) is a non-linear classifier. To assign a class to an unknown feature vector  $\mathbf{x}$  (extracted from a ROI),  $k$  feature vectors, out of a set of  $N$  training feature vectors  $\{\mathbf{x}_i; i = 1, \dots, N\}$ , are identified as the nearest neighbors to the unknown  $\mathbf{x}$ . Each one of the *k nearest neighbors*,  $\mathbf{x}_i$ , belongs to a corresponding class,  $\mathcal{C}_i$ , where the number of classes, for the application of detecting MCs, is two (*normal* and *abnormal*). Out of the *k nearest neighbors* to  $\mathbf{x}$ , the number of *nearest neighbors*,  $k_i$ , that belong to class  $\mathcal{C}_i$  ( $i = 1, 2$ ), are identified, where  $k = k_1 + k_2$ . The class, assigned to  $\mathbf{x}$ , is the one with the largest  $k_i$ . To avoid a tie between two classes,  $k$  must be an odd number. For a deeper and broader treatment of kNN the reader can consult [53].

### 1.4 Support Vector Machine (SVM) classifier

A *support vector machine* (SVM) is an optimal classifier which is geometrically represented by a separating hyperplane which is the furthest away from each class after training this classifier with labeled data (*supervised learning*). The *SVM*, used in this work, used a *Gaussian Kernel function*, with (1) one output node, which provides two possible outcomes, corresponding to two different classes (*micro-calcification* or *abnormal region, normal region*), and (2) four input nodes according to the size of the feature vector used. For a deeper and broader treatment of SVM the reader can consult [54].

### 1.5 Summary

This section mentioned the relevance of breast cancer worldwide. Typical processing time for the mammography test and for an expert to carry out the screening process to

then proceed to the diagnosis. Also, the most important characteristics of mammograms and the main databases were presented. Then, the definition of a microcalcification and its main physical characteristics were briefly presented. Finally, the most relevant works related to the segmentation and/or detection for microcalcifications were mentioned.

This dissertation is organized in four chapters: 1 introduction and previous relevant work about the topic; 2 problem statement, objectives, material and methods; 3 presents results and 4 presents conclusion, discussion and future work of this dissertation.



## Methods

---

### 2.1 Problem Statement

A 2014 OECD Mexico's report mentions that there are 689 mammography units and that 6.1%, of those units, are mobile to reach locations where there are no hospitals or where its access is difficult [55]. This number of mammography units means that there are 11 mammography units per million women. Meanwhile, countries as Austria, USA, France and Italy have 100, 89, 87 and 86 mammography units per million women, respectively [56]. Furthermore, the number of radiologists is an important issue for detection of breast cancer. For example, Mexico has 124 radiologists with specialty in mammograms [57] and 18.28 million women between 40 to 69 years old, age recommended to get a screening mammogram [58], [59]. Which means that there are close to seven radiologists, specialized in mammograms, per million women. The Table 2 summary the data collected in five different countries.

*Table 2. Number of radiologist and mammography units in five different countries.*

Country	Total number of mammography units	Mammography units per million women	Total number of radiologists specialized in mammography	Radiologist specialized in mammography per million women
Austria	420	100	150	36
USA	13,552	89	NA	NA
France	2,700	87	NA	NA
Italy	2,560	86	1147	38
Mexico	689	11	46	7

In the U. S. A., a mammogram study is completed in 15 minutes [6], it takes from one to two hours to interpret the mammogram by a technician, and 5 to 7 days to get the final results by the radiologist [7] This delivery time is mainly because radiologists,

specialized in the analysis of mammography, are fewer compared with the number of mammograms to analyze.

The problem to segments/locates microcalcifications has not yet been solved. This is mainly because of the size of microcalcification; and the fibro-glandular density of a given breast. Algorithms proposed in the state of art have not solved due to low resolution of the screen film mammography. Another problem is the variation of resolution causing to retrain and/or change significant parameters to detect MCs in different databases. Current approach has been to standardize resolution by decreasing size; thus, loosing resolution and possibly making impossible to detect the smallest MCs. From the state-of-the-art review there is no evidence that tests included enough MCs in a high-density breast since it is easily confused with the background, and in general do not specify if the test set included subtle MCs and how many.

Micro-calcification lesions are difficult to detect by human vision because the size of micro-calcification and a trained human vision can distinguish 30 shades of gray with difficulty [60]. For this reason, the *false positive rate* of the radiologist is reported as 15% [45] and the *false negative rate* as 20 % [61].

From medical point of view, when a CAD system is applied to detect lesions for screening is susceptible to errors, like false positive or false negative. In a review of CAD systems, their conclusion is that 50 out of 100,000 incremental cancer cases detected from screened mammograms by CAD systems, but generate 970 per 100,000 unnecessary biopsies this means an incremental recall of healthy women of 1190 per 100,000 [62].

Computer-aided detection (CAD) for mammography is a helping tool that can accelerate reading and help increase diagnosis' accuracy.

There are various studies that revised the efficacy of CAD. CAD plus single reading usually shows an increase in sensitivity and/or cancer detection rate, meanwhile there is no significant difference when comparing with double reading by radiologists. Many studies also report an increase in recall rate when adding CAD [63].

In a Breast Cancer screening programme there are two main possibilities. After the first reading use another blinded radiologist and the other possibility is use CAD for a second reading, as shown on Figure 6

Also, in the acquisition of the image have been occupied different types of enhancement algorithms. These algorithms are frequently included in the preprocessing stage.

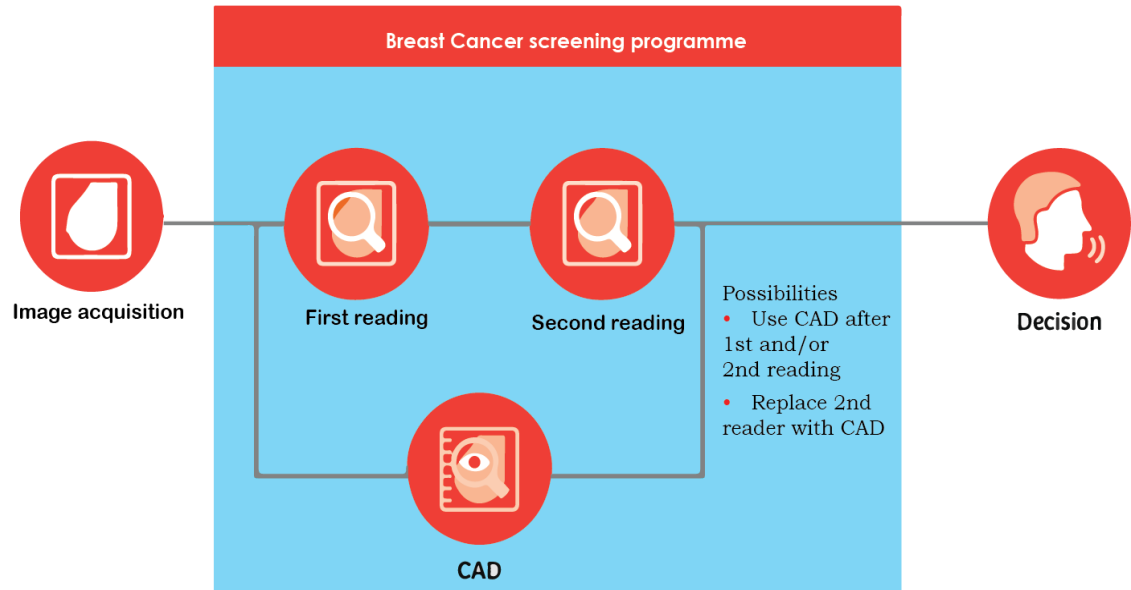


Figure 6. The two most common breast cancer screening programme

Other challenges are the resolution of some screen films that are digitalized at 0.2 mm per pixel. Hence, it is highly uncertain to say anything in areas of 2x2 or 3x3 pixels to detect microcalcification of size of 0.5 mm. Also, if the resolution changes, the training step must be performed again on works that use any kind of training.

Until now it is estimated that 98%, of the reviewed state of art, test the CAD system with one or two public databases and 87% their test sets are sub-images manually obtained by segmentation with no specified procedure.

Given these, a proposed solution is to design an algorithm to screen mammograms with the following features:

- Microcalcification segmentation/detection

- Directly uses resolution on and better or equal than 100 micron per pixel
- Uses datasets of Digitized film screen, and Full field digital mammograms
- Algorithm provides areas with high probability to have lesion and/or cluster of lesions

The above characteristics should help reduce the 15% FPR [45] and the 18% FNR [64] by the radiologist, as well as their diagnostic time. As it is shown in the Figure 7.

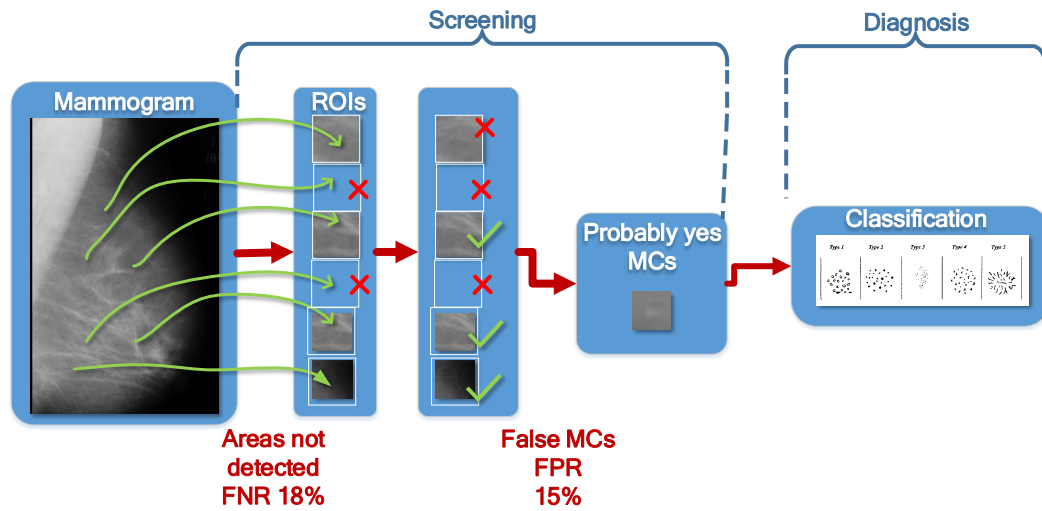
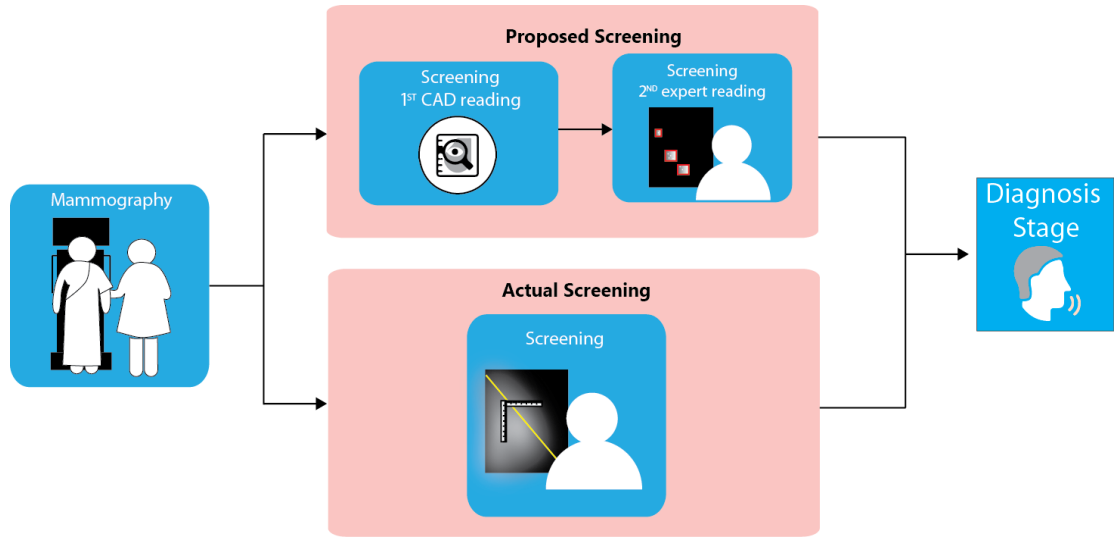


Figure 7. Human error in the analysis of a mammogram

One possible way to solve this is imitating the process that a radiologist specialized in mammograms does. It means extracting the general features that he/she observes to identify a MC independently of the image source, resolution or mamma type.

A CAD algorithm will help the mammogram specialized radiologist to identify easier and faster these lesions, decreasing the workload per mammogram, and possibly improving his/her accuracy, by presenting only the regions of interest with possible MCs to be diagnosed by the radiologist, relieving them from the work to screen all the mammogram, and concentrated only on the areas that possibly contain MCs, as is show in Figure 8.



*Figure 8. Proposed and actual screening process.*

For the aforementioned reasons the development of automatic systems for pre-diagnosis of breast cancer performs a quick assessment of a mammogram and to indicate if there is any type of micro-calcification that requires the intervention of a specialist. In addition, the algorithm of detection of micro-calcifications must be simple to facilitate its subsequent mass deployment. The simplification of early and preliminary diagnosis will be supported by algorithms with low computational resources. In addition, the number of radiologists, who are specialized in mammography, is much lower than the number of women with breast cancer. For these reasons, this work proposes an algorithm, which detects micro-calcifications on digital/digitized mammograms based on morphologic processing, supervised learning and very small set of features. These arguments encourage the implementation of devices for autonomous diagnostic that will help to reduce the number of women who attend a specialist without apparent breast cancer and, most importantly, to detect early risks of breast cancer by finding the presence of MCs on mammograms and encouraging patients to follow specialized treatment that will give them best prognosis.

## 2.2 Dissertation Goals

### 2.2.1 General Goal

Design an algorithm that can detect isolated and clustered microcalcifications in diverse breast density, and different image resolution. The algorithm should be competitive with state of art results.

### 2.2.2 Specific Goals

- Use natural characteristics of a microcalcification observed on a mammogram image
- Use at least two public databases of different resolution with ground-truth for testing
- Flexible to breast density
- Parameterized for mammograms with different resolution
- Algorithm should consider cues given by mammography atlases

### 2.2.3 Dissertation Contribution and Organization

Expected contributions of this research work may be summarized in the following points:

- Intensity model for microcalcifications
- Application of a measure of contrast for MCs, by using Weber's formula.
- Results will be generalized for different:
  - Resolution
  - Breast density
  - Contrast values for obvious, regular, and subtle MCs.

## 2.3 Material and Methods

### 2.3.1 Mammogram data sets

Two of the most popular public data sets in the scientific literature are used for this research, the *Mammographic Image Analysis Society Digital Mammogram Database*, also known as MIAS [17], and the *Digital Database for Screening Mammography*,

DDSM [18]. The first data set contains 322 medio–lateral (MLO) mammograms digitized at a spatial resolution of  $50 \frac{\mu m}{pixel}$  and  $8 \frac{bits}{pixel}$ . However, this database has been reduced  $200 \frac{\mu m}{pixel}$  and padded so that every image is 1024 X 1024 pixels, this reduced database is named mini-MIAS and is widely used. Images, from this data set, present two categories of *abnormality*, 207 *normal images* and 20 images with *micro-calcifications*. Images, with MCs, are characterized by defined areas on the *Ground Truth* (GT). There are three MIAS images with micro-calcifications, but without defined areas in the GT. Images with micro-calcifications are provided along with their corresponding GT while normal images were not analyzed so that they do not have GTs. These two image categories are also sub-classified in terms of *breast density type*; *fatty*, *fatty-glandular*, and *dense*. The ground truth specifies information regarding *Regions of Interest* (ROIs) which are *clusters with micro-calcifications*. The set of 20 images, with specified ground truth, contains a total 25 regions of interest with *micro-calcification clusters* or *abnormality clusters*. A ground truth cluster is identified by (1) a *set of coordinates* ( $x, y$ ) where each set of coordinates corresponds to the center of an abnormality cluster; and (2) a *region radius* (in pixels) which represents a circle enclosing the abnormality. A complete description of the MIAS data set, based on breast density, is shown in Table 3.

Table 3. Description of MIAS data set in terms of breast density.

MIAS database				
	Fatty	Fatty-glandular	Dense	Total
Number of images with clusters of microcalcification	5	6	9	20
Images with isolated microcalcifications	1	1	1	3
Number of clusters in GT Images	5	6	14	25
microcalcifications regions	50	97	121	268
Images without microcalcification clusters	66	65	76	207

The DDSM data set was digitized by four different scanners, DBA M2100 ImageClear ( $42 \frac{\mu m}{pixel}$  and  $16 \frac{bits}{pixel}$ ), Howtek 960 ( $43.5 \frac{\mu m}{pixel}$  and  $12 \frac{bits}{pixel}$ ), Lumisys 200 Laser ( $50 \frac{\mu m}{pixel}$  and  $12 \frac{bits}{pixel}$ ), and Howtek MultiRad850 ( $43.5 \frac{\mu m}{pixel}$  and  $12 \frac{bits}{pixel}$ ). It is organized into *cases* and *volumes*. A *case* is a collection of images and information corresponding to one mammography exam for one patient. A *volume* is a collection of cases, collected for purposes of distribution ease. The data set has 2,620 cases available in 43 volumes from which there are 106 mammograms with micro-calcifications. This database used the information related to this data set as shown Table 4. This Table does not contain the same type of detailed information as Table 3 because DDSM images in the database do not include breast density type. In this work we used the CBIS-DDSM (Curated Breast Imaging Subset of DDSM) is an updated and standardized version of the DDSM. The CBIS-DDSM collection includes a subset of the DDSM data selected and curated by a trained mammographer [65], [66]. The images have been decompressed and converted to DICOM format. Updated ROI segmentation and bounding boxes, and pathologic diagnosis for training data are also included. For this case the GT is identified pixel level boundary of the lesion

*Table 4. Description of DDSM data set in terms of abnormality.*

	DDSM	
	Abnormal	Normal
Images	29	20
Microcalcifications regions	114	114



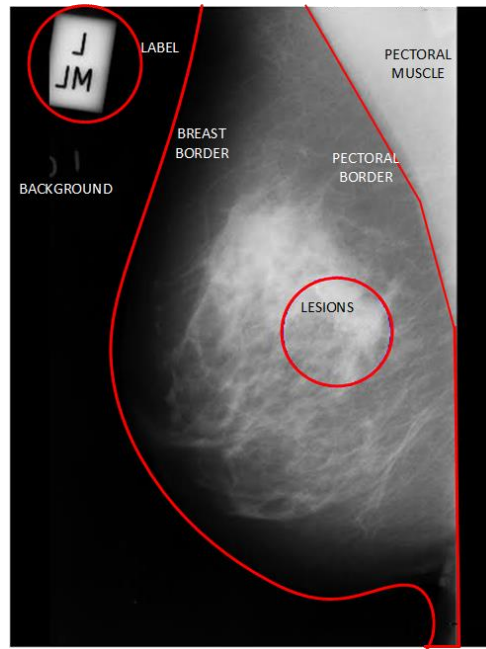


*Figure 9. Principal regions from a mammography*

A typical mammography has different parts, as shown in the Figure 9. As it can be observed in the figure it is necessary to remove the labels and the background in a preprocessing stage. It should be mentioned that there are two types of background, the background that is located next to the edge of the breast (on digitized mammograms regularly it is not completely black, there are exceptions like in database type FFDM) and the background that is located on the side of the pectoral muscle (the intensity value in this case is 0 ). Also, it can be observed that the background is blurred with the edge of the breast, making it difficult to define exactly the edge of the breast. This removal process is known as breast extraction. One of the regions that has taken relevance is the area of the pectoral muscle. This is because in a CAD, the existence of the pectoral muscle may mislead the diagnosis of cancer due to its high-level similarity to dense tissue breast. In addition, some other challenges due to manifestation of pectoral muscle in the mammogram data include inaccurate estimation of the density level in the breast region. Regardless of improvement of imaging technology and algorithms, accurate segmentation of the breast boundary and detection of the pectoral muscle are still challenging tasks. Obtaining its boundaries leads to useful information about the

position of the breast and its orientation as well as the general intensity of the gray levels in the image. These steps are shown in Figure 10

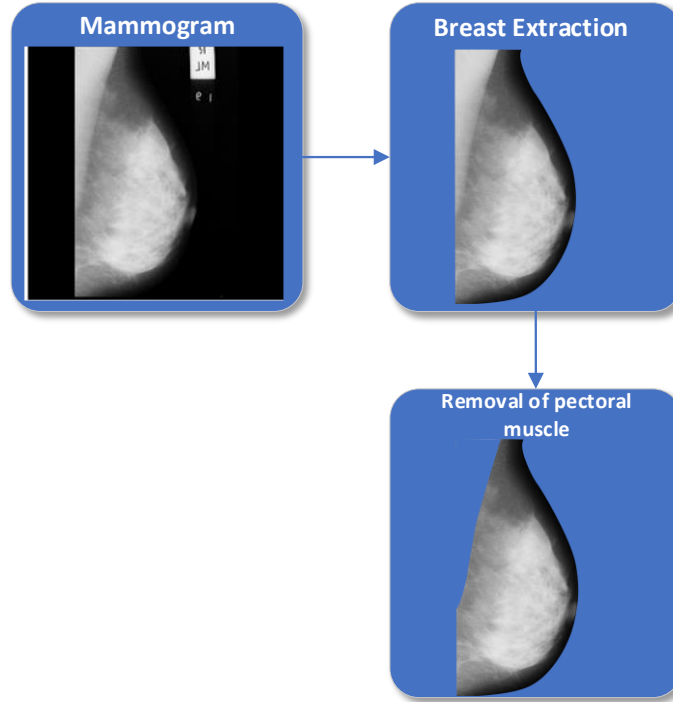


*Figure 10. General pre-process for breast extraction*

Extraction of abnormality clusters, from a GT image, is accomplished by a radiologist, who specifies (1) the image coordinates  $(x, y)$  of the center of each abnormality cluster, and (2) an approximate radius, in pixels, of a circle enclosing an abnormality cluster, as it is shown in Figure 11. In the proposed approach, rather than enclosing an abnormality cluster by a circle (central part of Figure 11), a square is used (right part of Figure 11), given that the search for individual micro-calcifications is performed by a scanning process that takes place on a rectangular area.

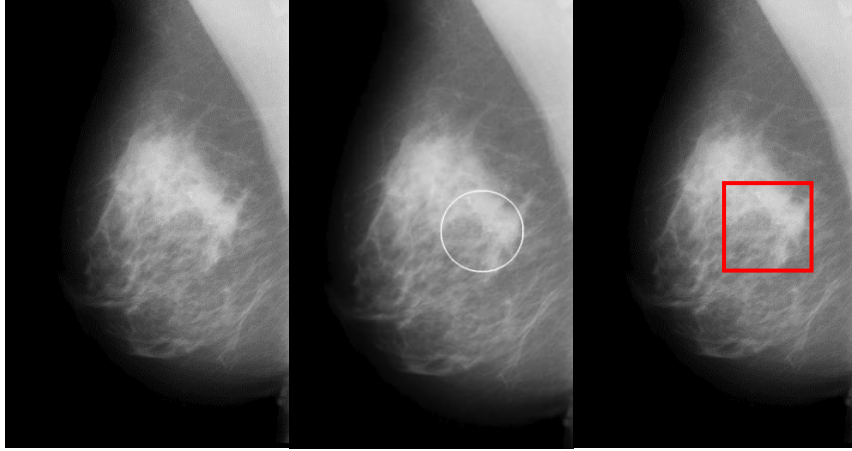


*Figure 11. Digital mammogram, from the MIAS data set, with one cluster of micro-calcifications.*

The general algorithm, which is shown in Table 5, is applied to images from any data set, MIAS or DDSM, and from any density group, fatty, fatty-glandular, and dense. The input to the algorithm is a GT image, which contains squares, where each square encloses a micro-calcification cluster. Thus, the size of the enclosing square depends on the size of the enclosed micro-calcification cluster. Each enclosed cluster might consist of one or more micro-calcifications. The command, for extraction of an abnormality cluster, is executed in the second line of the general algorithm, listed in Table 5. Each ROI or micro-calcification candidate, on the abnormality cluster, must be detected and extracted individually (fourth line of the general algorithm, listed in Table 5).

Table 5. General algorithm for extraction of ROIs from ground truth images.

---

<b>input</b>	: data set image with micro-calcification clusters
<b>output</b>	: set of image patches corresponding to micro-calcification candidates

---

```

1  Begin
2  extraction of rectangular regions enclosing abnormality clusters from ground truth image
3      for each cluster
4          extraction of image patch with a micro-calcification candidate
          end
      End

```

---

## 2.4 Microcalcification Segmentation

In this work we focus on the detection of MCs as the means for early diagnosis. A simple method to segment an MC is the thresholding. This technique has been used by some works as, [67]–[72], at least on one stage of the process. However, all microcalcifications are not visually equal. This is due that the intensity of the tissue that surrounds the MC could be from high to low compared with the intensity of MC. The breast tissue is categorized from mostly fatty tissue to extremely dense tissue with very little fat in Figure 12 shows samples for the 4 breast density types. In addition, for the first time in more than 20 years of regulating mammography facilities, the agency is proposing regulations that would help improve the quality of mammography. It is now a federal law develop breast density reporting language that must be included in patient letters and health provider reports [73]

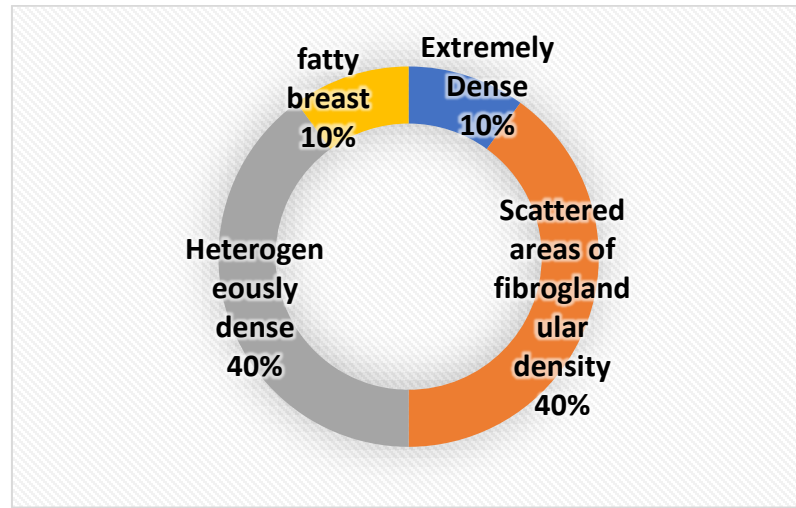


Figure 12.- Breast density variety [74]

Therefore, automatic segmentation of microcalcifications (MCs) can be a challenging task, mainly due to the high breast density (Extremely Dense and Scattered areas of fibro-glandular). A high-density breast area makes very challenging the observation of microcalcifications, given the low contrast of the MC area to the background. Therefore, it is convenient to classify the type of microcalcification according to tissue that surrounds it. This research work first approached this by selecting a set of methods and comparing them in a set of cases that include **different** tissue densities. we identify three: *subtle*, *obvious* and *cluster* of MCs, as they are shown in Figure 13.

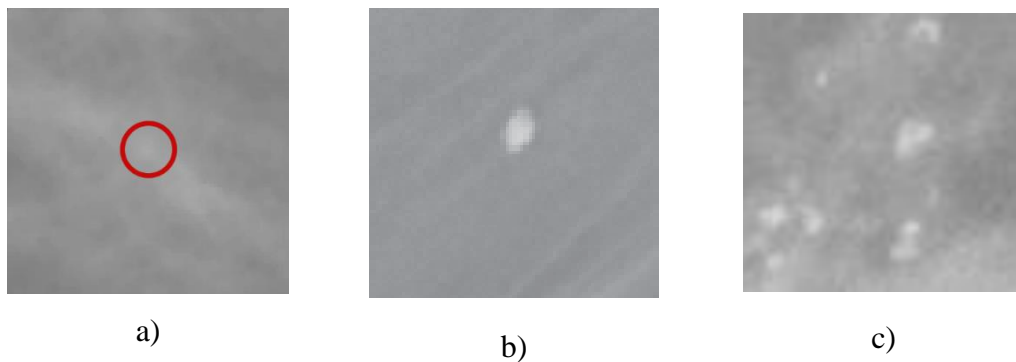


Figure 13. Classification of MCs according to their surrounding tissues; a) Subtle, b) obvious and c) Cluster type.

To measure the different contrasts of obvious and subtle MC's. There are several measures of contrast, one of the most common measure is the Weber contrast [75], that is defined as:

$$C_M = \frac{I - I_b}{I_b}$$

Where  $I$  is the intensity of the center pixel or the mean pixels of the foreground, and  $I_b$  the intensity of one pixel consider as the background or the mean of some pixels consider as the background. From the analysis of several microcalcifications the range of the values for subtle, normal and obvious groups was estimated. For the subtle-group, the Weber contrast is under or equal to 0.1; normal MCs have an interval above 0.1 but under or equal to 0.2 and for the obvious group values above 0.2. Table 6 summarizes the contrast level range for this particular measure.

A sample of some microcalcifications for each group and the respective Weber contrast values, are shown in Figure 14. As can be seen in this image the MCs that are visible, have  $C_M$  values above 0.1, that means MCs classify as normal or obvious. In the other hand, when the MC is not visible, as in Figure 14 a), the  $C_M$  is under or equal to 0.1.

*Table 6. Range of values for weber contrast measures of different groups*

<b>Type MC</b>	<b><math>C_M</math></b>
Subtle	$\leq 0.1$
Normal	$0.1 < C_M \leq 0.2$
Obvious	$> 0.2$

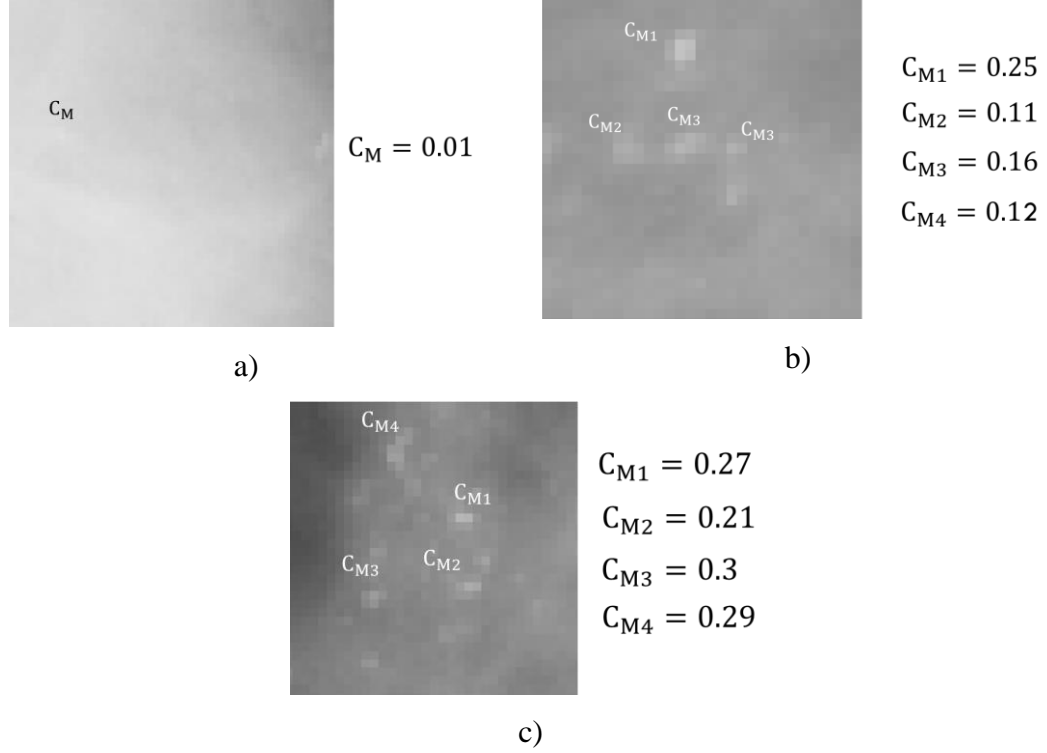


Figure 14. Examples for some Weber contrast values of a) subtle b) normal and c) obvious groups.

From a literature review [76] [77] the most commonly used thresholding algorithms are proposed by [78], [79], [80], [81], these threshold methods are Intermodes, Kittler and Illingworth, Entropy and Otsu respectively.

As part of the research work, a review was published on a paper in 13th International Conference on Electrical Engineering, Computing Science and Automatic Control (CCE), Mexico, City, 2016, Mexico named “*Thresholding Methods Review for Microcalcifications Segmentation on Mammography Images in Obvious, Subtle, and Cluster Categories*” [82]. This paper compares four commonly used thresholding techniques to segment mammography images sections divided in three groups: *obvious*, *subtle* and *clusters*; due to their microcalcification context. The purpose of this paper it is to show which technique has a better performance for mammography images.

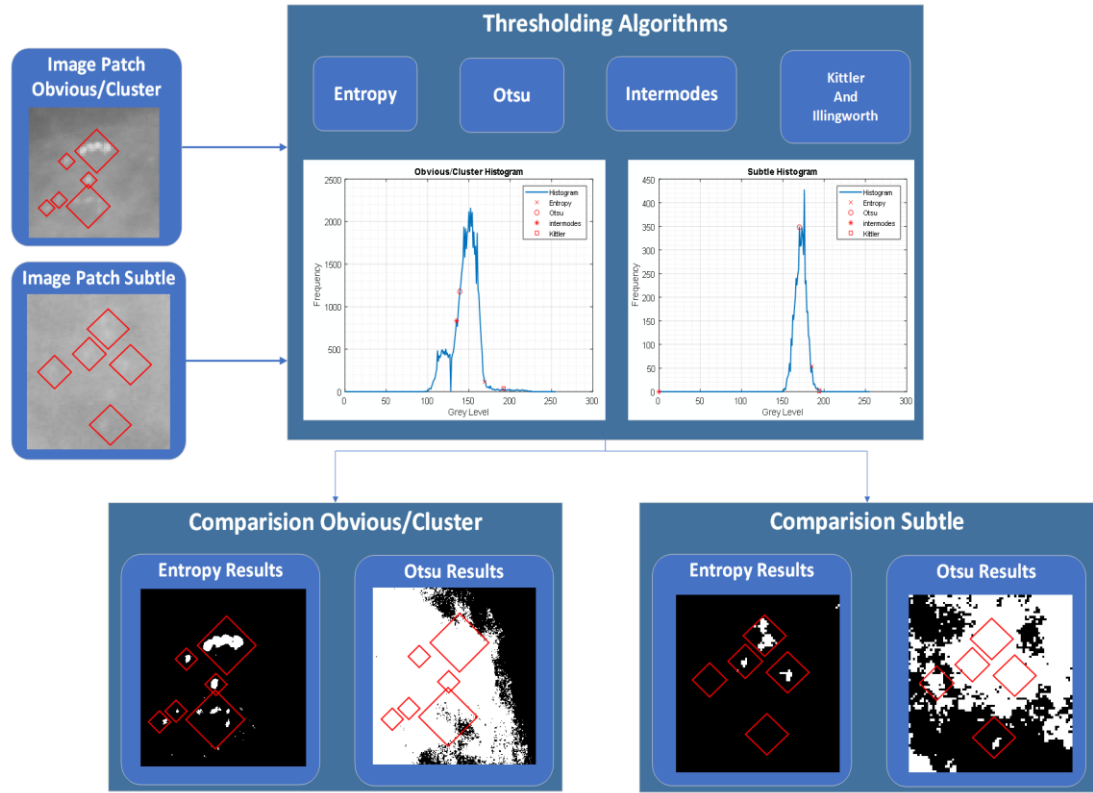


Figure 15. General process in the Microcalcifications segmentation

Figure 15 shows the general process used for the segmentation of MCs. That is, from an image patch, defined in detail in the corresponding paper, different threshold values are generated using the 4 methods. Also, Figure 15 shows the histograms of each image and their corresponding threshold points for each method. Then, a comparative analysis is performed to decide how many MCs were detected for each method. In a special case, here the Otsu method is compared because it is the most used in the literature, and the entropy method, that gives better results. The results from the reported paper shows that the Entropy method is better than twice as much the Otsu method in both obvious and subtle MCs. Table 9 of the results chapter each of the methods with their respective results is reported in detail.



## 2.5 Microcalcification modelling and classification

A microcalcification region is 21 X 21 pixels (ROI), regions were extracted from both databases. The size of the ROIs is due that the resolution of the mini-MIAS database is 200 microns and we want a MC to have enough tissue around it to be able to distinguish it, knowing that the maximum size of an MC is 1 mm. Also, this size helps in case of a cluster. This data set of ROIs with MCs candidates are known as true positives. In addition, it is necessary to have other data set of ROIs, known as true negatives, which are regions that do not contain any type of MCs. The size of these regions should also be 21 X 21.

Table 7 describes the general steps of an algorithm to generate this data set. A normal image, with a large breast region, is randomly selected at each loop of the for cycle. From each randomly selected normal image (command executed in the third line of the general algorithm listed in Table 7, a candidate is randomly extracted (command executed in the fourth line of the algorithm listed in Table 7. Each normal image is tagged with an image number, and to generate a set of randomly selected normal images,  $n$  random *image tag numbers* are generated by means of a *discrete uniform probability density function*,  $f_x(x) = \frac{1}{m}$ ; where  $x \in \{1, 2, \dots, m\}$  is an *image tag number*; and  $m$  is the total number of images from each type of mammogram density. Parameters,  $(n, m)$ , are  $(n = 121, m = 76)$ ,  $(n = 97, m = 65)$  and  $(n = 50, m = 66)$  for *dense, fatty-glandular* and *fatty* mammograms, respectively. The criteria to choose a value for  $n$ , is to have the number of candidates, which are MCs, equal to the number of candidates, which are not, for each mammogram density. According to Table 3, row for microcalcifications regions, there are 121 MCs in 9 dense mammograms, 97 MCs in 6 fatty-glandular mammograms, and 50 MCs in 5 fatty mammograms.

Similarly, one pair of random numbers,  $(r, c)$ , is generated for each randomly selected image. Parameters  $r$  and  $c$  are used as the coordinates of the center of a randomly chosen ROI, of 21 X 21 pixels, on the corresponding randomly chosen normal mammogram.

Table 7. Random generation of a set of  $n$  micro-calcification candidates from the set of normal images without abnormality clusters identified by the radiologist.

<b>input</b>	: data set of normal images without abnormality clusters identified
<b>output</b>	: data set of image patches of $21 \times 21$ pixels
<b>Begin</b>	
1	<b>for</b> a given number $n$ of ROIs required
2	random selection of a normal image along with a set of image coordinates $(r,c)$
3	extraction of an image patch with center at $(r,c)$ and size of $21 \times 21$ pixels
4	<b>end</b>
<b>end</b>	

## 2.6 Extraction of micro-calcifications candidates from abnormality clusters

Extraction of micro-calcifications, from an abnormality cluster, is separated into different stages, for *segmentation* (contour detection, noise suppression, sharpening), *binarization*, *feature extraction*, and *classification* as it is depicted in Figure 16.

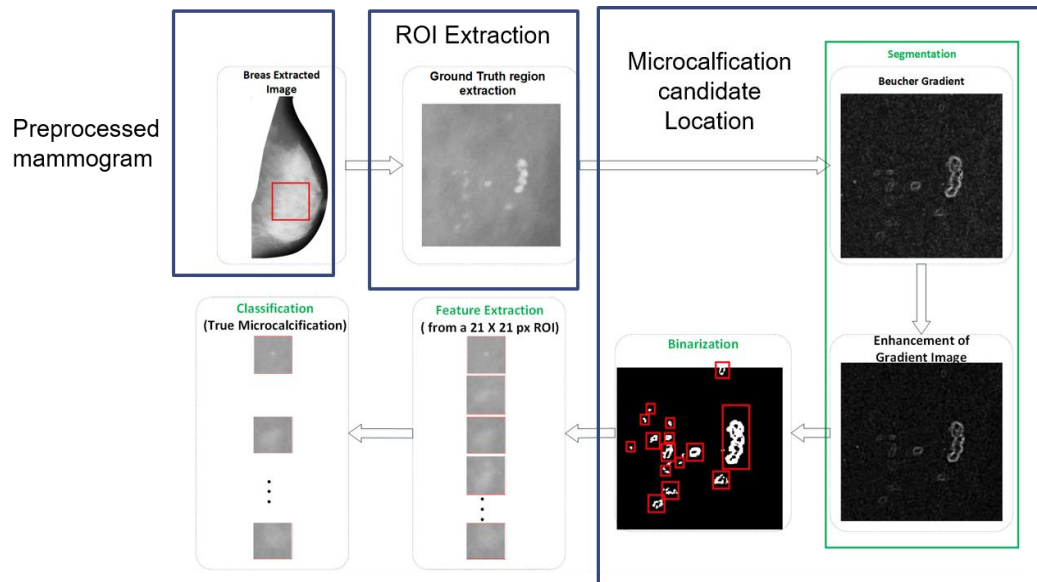


Figure 16. Different stages for detection of micro-calcifications, segmentation, binarization, feature extraction, and classification

A *mammogram* (upper left corner in Figure 16) is a digital grayscale image which is denoted as a function  $f(r, c)$  on the two-dimensional discrete space  $(r, c) \in \mathbf{Z}^2$ , where  $r$  stands for row and  $c$  stands for column.

*Morphological processing* [83] of grayscale images is used for binarization of images of interest as well as detection of regions of interest. From the upper central part of Figure 16, which shows an abnormality cluster, it is observed that brighter ROIs (such as micro-calcifications) correspond to local maxima of the function,  $f_{max}$ . To achieve segmentation of micro-calcification candidates, bright regions, corresponding to local maxima of  $f(r, c)$ , are emphasized; while the background, corresponding to local minima of  $f(r, c)$ , is removed.

Because of the fact that *dilation* of gray-level images enhances bright regions and suppresses dark regions while *eroding* enhances dark regions and suppresses bright regions, where the area of the suppressed region is smaller than the area of the specified *structuring element*  $b(r, c)$ , both operations are combined, through the use of the high-pass filter, *Beucher Gradient* [84], for extraction of local maxima (micro-calcification candidates) and removal of local minima (background). The *erosion* of a gray-level image  $f(r, c)$  by a *structuring element*  $b(r, c)$  at location  $(r, c)$  is obtained by selecting the minimum value of  $f - b$  inside the region of intersection over which both functions  $f$  and  $b$  are defined according to

$$[f \ominus b](r, c) = \min_{(x,y) \in b} \{f(r - x, c - y) - b(x, y)\}. \quad (1)$$

The *dilation* of a gray-level image  $f(r, c)$  by a structuring element  $b(r, c)$  at location  $(r, c)$  is defined by finding the maximum value of  $f + b$  inside the common region between both, function  $f$  and structuring element  $b$ , according to

$$[f \oplus b](r, c) = \max_{(x,y) \in b} \{f(r-x, c-y) + b(x, y)\}. \quad (2)$$

By considering flat structuring elements with zero entries, *eroding* or *dilating* of a gray-level image with a structuring element consists in finding the *minimum* or *maximum* value of the image inside the region bounded by the intersection of the image and the structuring element.

The morphological gradient, known as *Beucher Gradient*, is the arithmetic difference between the dilated and the eroded version of the gray level image of interest  $f(r, c)$ , by a *structuring element*  $b(r, c)$ ,

$$g(f(r, c)) = [f \oplus b](r, c) - [f \ominus b](r, c) \quad (3)$$

where this morphological operation represents the maximum variation of gray level intensities within a pixel neighborhood. The result of applying Beucher Gradient on a mammogram is shown in the upper right part of Figure 16.

To improve the quality of the filtered image, a  $3 \times 3$  *median filter* is applied, a non-linear filtering technique to remove noise while preserving edges. This filtering technique runs in a pixel-by-pixel fashion, replacing each pixel by the *median* of neighboring pixels inside a  $3 \times 3$  window. To enhance edges, a process, called *unsharp masking*, is applied, where a *smoothed* version of the image (Gaussian low-pass image),  $f_{smooth}(r, c)$ , is subtracted from the original image, subtracting away the low-frequency components of the signal, and yielding the high-frequency content,

$$f_{high-pass}(r, c) = f(r, c) - f_{smooth}(r, c) \quad (4)$$

where the standard deviation of the Gaussian low-pass filter, was set to 2, and the high-pass image component can be used for sharpening by adding it to the original image. Thus, the complete *unsharp masking* operator is given by

$$f_{sharpen}(r, c) = f(r, c) + k \times f_{high-pass}(r, c) \quad (5)$$

where  $k$  is a scaling constant, set to 0.7. The result of applying *median filtering*, followed by *unsharp masking* is shown in the lower right part of Figure 16.

The segmentation stage (morphologic processing, median filtering, unsharp masking) is essential to the success of micro-calcification detection since this stage reduces background variations, noise, and enhances edges of ROIs or candidates. Then, *thresholding* is applied to generate a binary image where ROIs are white, and the background is black, as it is depicted in the lower central part of Figure 16. By analyzing the histogram of multiple  $21 \times 21$ -pixel image patches, with segmented micro-calcifications, the threshold value, for binarization, is established to the 90 % of the highest gray value of the enhanced GT region of interest.

One impairment of binarization is that remaining noise might be misclassified as a candidate to micro-calcifications. To reduce the likelihood of the occurrence of these misclassifications, ROIs, with radii smaller than 0.1 mm, are eliminated using *opening* with a disk-like structural element of 0.2-mm diameter. The reason for choosing a structuring element of 0.2-mm diameter is based on the consideration that the diameter, of the smallest micro-calcification, is 0.2 mm (4 pixels for the MIAS). The *opening* of a binary image  $f(r, c)$ , by a structuring element  $b(x, y)$ , is given by  $f \circ b = (f \ominus b) \oplus b$ , and it eliminates objects smaller than the structuring element. Resolution of digital mammograms, for both data sets, is 50  $\mu\text{m}$  per pixel. Thus, the size of the structuring element, in pixels, is  $\frac{0.2 \text{ mm/diameter}}{50 \mu\text{m/pixel}} = 4 \frac{\text{pixels}}{\text{diameter}}$ .

Another consideration is that the diameter, of the largest micro-calcification, is 1 mm. Thus, the size of the circle, which encloses a candidate to micro-calcification, is  $\frac{1 \text{ mm}/\text{diameter}}{50 \mu\text{m}/\text{pixel}} = 20 \frac{\text{pixels}}{\text{diameter}}$ , and the area of the corresponding square is chosen as  $21 \times 21$  pixels. The extraction of the set of candidates to micro-calcification or ROIs (output of the general algorithm listed in Table 1), from an abnormality cluster, is shown in the lower left part of Figure 16. Each candidate is contained on a  $21 \times 21$  image patch. The center of the patch is established at the position of the highest gray level value of the ROI.

To recover the complete shape of candidates, at all locations of interest, an algorithm for *extraction of connected components* is used. Another motivation for extraction of connected components is to assign a label to each region of interest for sub-sequent automatic extraction of *properties* from each labeled ROI, mainly the position of the highest gray level value inside the region. Let  $f(r, c)$  be a binary image containing one or more connected components, then another image segment  $f_0(r, c)$ , of the same size as  $f$ , is initialized with all its elements being zero, corresponding to black background, except those elements at locations where it is known there are white connected components in  $f_0(r, c)$ , which is set to one. The goal is to start with the initial image  $f_0(r, c)$  and eventually to extract all the connected components by performing the following iterative process;

$$f_k = (f_{k-1} \oplus b) \cap f \quad (6)$$

Where,  $b(r, c)$  is a suitable structuring element for extraction of connected components. The iterative process is finished when  $f_k = f_{k-1}$  with  $f_k$  containing all the labeled connected components.

To compare works that detect microcalcifications, it is essential to measure the efficiency of the algorithms. To perform an evaluation is necessary to use measures of efficiency previously in other works. These are: the area found by the algorithm and intersection with the GT as true positive (TP), and the area found but does not intersect any GT area as false positive (FP). Additionally, the area that is not in GT and is not given by the algorithm as true negative (TN). Finally, the area that is in GT but was not found by the algorithm as false negative (FN). From the literature review, the way these measures are found varies, Table 8 points out some of the differences.

*Table 8. State of the art Comparison diversity*

Ref.	Decision(s) to define TP, TN, FN and FP
[85]	Overlap larger than 50% by human observation
[86]	Area overlap measure (AOM) automated, ideal value equal to 1. Draw a bounding circle to the detected MCs, More than 2/3 bounding circle of the MC clusters are overlapped with
[25]	ground truth becomes a true-positive (TP). For clusters area, if we detect at least one it is as TP. For mammograms MC's, if we cannot detect out any MC's, we consider it as true negative (TN)
[24]	Completeness, CM, correctness, CR and quality, ACC
[87]	Confusion matrix

From the above, it can be observed that one of the main problems is the comparison of results between different databases. For example, the GT in the MIAS database identifies lesions using a circle while DDSM does so by surrounding the pixel-to-pixel lesion, meaning that the contour can be irregular. Also, in the DDSM database, whether the MCs are very small then the GT points out them using only the coordinates of one pixel. In addition to this, the form of comparison between different algorithms varies as can be seen in the Table 8.

Knowing that the MC can be classified in the categories previously mentioned; it is useful to visualize a micro-calcification in the three-dimensional space, as a gray level function of coordinates  $(x, y)$ , as it is observed in Figure 17. This three-dimensional reconstruction provides an approximation of the projection of an actual micro-calcification into a set of intensity values on a digital mammogram through absorption of X-ray radiation. The three-dimensional reconstruction of a micro-calcification consists of a prominent peak in relation to local surroundings on the mammogram. Thus, it is feasible the modeling of a micro-calcification based on a *set of surface levels*.

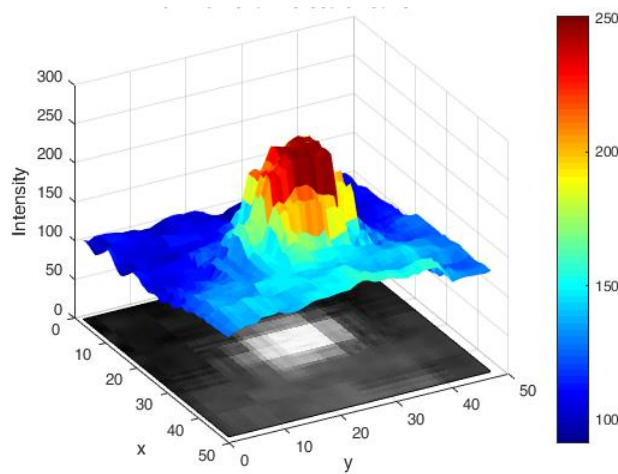
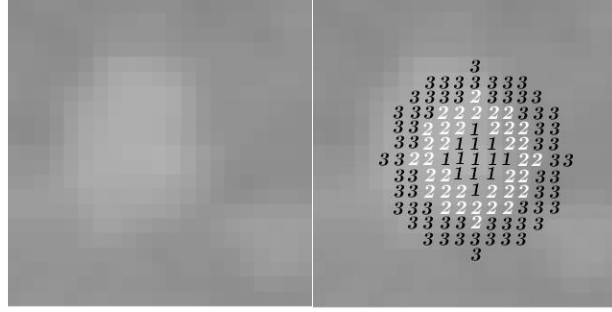


Figure 17. Three-dimensional visualization of one micro-calcification on a digital mammogram.

The results of this work were published in the Journal of Medical Systems titled “False Positive Reduction by an Annular Model as a Set of Few Features for Microcalcification Detection to Assist Early Diagnosis of Breast Cancer” [88]. The work reported in this paper proposes to extract only four features from a candidate. To accomplish this, information is obtained from three different surface levels assigned to each ROI, by using a mask, which contains the distribution of these surface levels. The left part of Figure 18 shows a ROI of 21 X 21 pixels and with its center at the maximum intensity value. Information, for each surface level of the ROI, is extracted by overlapping the ROI with a mask which shows the distribution of each of the three surface



levels. The right part of *Figure 18* shows, the mask along with the distribution of each surface level. It can be seen that the surface level distribution consists of three concentric annulus (ring-shaped object) with its respective radii  $R$ ,  $R + 2$  and  $R + 4$ . This work arrived to having  $R = 3$ , by considering known sizes of micro-calcifications at 50 microns per pixel and observing the corresponding method performance. Each annular region,  $A_{annulus}$ , provides information of interest regarding each surface level. Each annular region is labeled by an integer number in the set  $\{1, 2, 3\}$ .



*Figure 18. Region of interest (left part) along with the corresponding mask of three surface levels (right part). Overlapping the ROI and the mask allows the extraction of information from different surface levels for sub-sequent feature extraction.*

After overlapping the mask with one ROI, information from the three annular regions is used for extraction of a four-entry feature vector,  $\mathbf{f} = [f_1, f_2, f_3, f_4]^T$ , according to,

$$f_1 = \max(A_{annulus1}) - \max(A_{annulus2}) \quad (7a)$$

$$f_2 = \max(A_{annulus1}) - \max(A_{annulus3}) \quad (7b)$$

$$f_3 = \text{mean}(A_{annulus1}) - \text{mean}(A_{annulus2}) \quad (7c)$$

$$f_4 = \text{entropy}(A_{\text{annulus1}}) - \text{entropy}(A_{\text{annulus2}}) \quad (7d)$$

where functions  $\max()$ ,  $\text{mean}()$ , and  $\text{entropy}()$  are the *maximum*, *mean* and *entropy* values, respectively, of the corresponding annular region intensity values. The *entropy value* is computed according to,

$$H = \left| - \sum_i p_i \log_2(p_i) \right| \quad (8)$$

where  $i \in [0, 255]$  is a *gray level value*, and  $p_i$  is the probability associated with gray level value  $i$ , i. e., the *probability density function* of an annular region.

The feature selection, in the proposed method, has the purpose of achieving low computational complexity and simplicity, and the additional purpose of being representative of the process of that a radiologist follows. In an ideal micro-calcification, the maximum intensity value is at the center of the MC enclosing region. It can be modelled as a Gaussian function. The first feature,  $f_1$ , represents the difference between the peak intensity value, in the first annular region, and the peak, on the second annulus. Ideally, if a micro-calcification exists, this difference must be greater than or equal to 1 pixel; otherwise, if a micro-calcification is not present, then the difference might be less than 1 pixel. This idea is similar for second feature,  $f_2$ , but in this case the difference values increases proportionally with the size of the MC. For the third feature,  $f_3$ , the mean value of each annulus is close to its maximum value. Then, the difference between first and second mean values must be greater than or equal to 1 pixel; otherwise, this difference is less than 1 pixel, when MCs are not present. Another feature is the entropy value. For each annular region the entropy value should be ideally close to zero. Thus, the difference of entropy values between the first and second annular regions should be close to zero. Meanwhile, when there are not MCs, the entropy value

should be greater than zero since background intensity values are characterized by containing *salt and pepper noise*.

Figure 19 shows in general the process for detecting and classifying MC. For the classification stage, two classifiers, KNN and SVM, were tested. The results of these classifiers are shown in the next chapter and for further details consult the published paper [88].

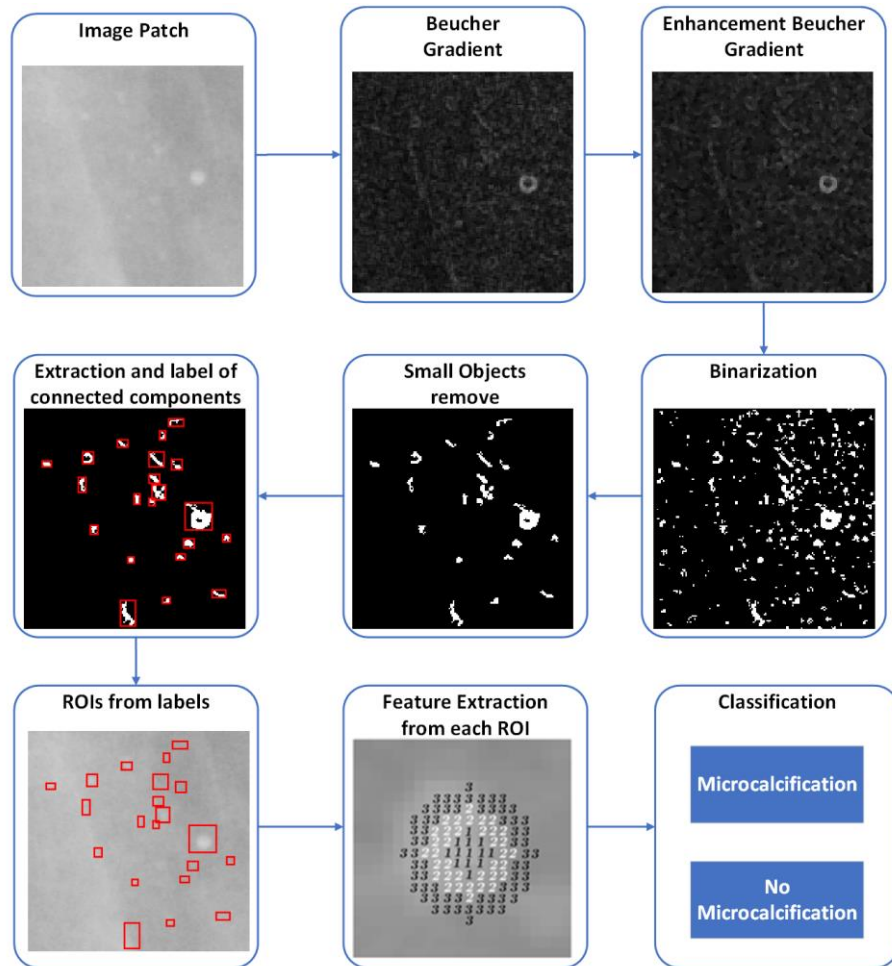


Figure 19. General process to detect and classify a MC

## 2.7 Summary

This chapter stated the problem that motivated this research work. The high workload of specialized radiologists who are experts in the screening process. Likewise, the objectives and contributions of this dissertation are presented.

Then, the most important characteristics of the main databases and their mammograms are presented. The images that were used in each of these databases are mentioned. Finally, it presents the most important aspects that were performed for the segmentation and detection of microcalcifications, such as the analysis of different thresholding methods and the creation of a model based on annular regions. The results of the methods and analysis presented in this chapter are described on the next Chapter.

## Results

---

### 3.1 Microcalcification segmentation results

This dissertation work introduces a new approach to the detection of MCs in mammograms. The first stage of this work is to understand the importance of early detection and how MCs are relevant at this stage. Important aspects of MCs were defined as their relation of intensity to the surrounding tissue. Thus, this help us defining the *subtle*, *obvious* and *cluster* groups. Separating them into these groups, the detection of MCs improves using a technique as simple as thresholding. The results of this part of the research are presented in Table 9, showing the different methods of thresholding that were applied and the corresponding results.

Table 9. Total result accordance to category and techniques

	Intermodes	Kittler	Entropy	Otsu	Total GT
Obvious	15	1	15	6	16
Cluster	39	13	56	23	79
Subtle	3	3	6	6	17
Total (MCs)	57	17	77	34	112
Total (%)	50.893	15.179	68.750	30.357	

### 3.2 Microcalcification model for detection

To compare works that detect micro-calcifications, it is essential to compare efficiency among different proposed methods. To evaluate the performance of the proposed method, *True Positive Rate* (TPR) or *sensitivity*, *False Positive Rate* (FPR), *specificity* and *accuracy* are used as figures of merit. TPR, also known as *sensitivity* or

*recall* or *detection alarm*, is the probability that the outcome of a diagnosis is positive given that the patient presents breast cancer, and it is given as,

$$TPR = \frac{TP}{TP + FN} \quad (9)$$

where *true positives* (TP) are those micro-calcifications correctly identified and *false negatives* (FN) are those micro-calcifications incorrectly rejected. *False Positive Rate* (FPR), also known as *false alarm*, is defined as the probability that the outcome of a breast cancer diagnosis is *positive* given that the patient is healthy according to

$$FPR = \frac{FP}{TN + FP} \quad (10)$$

where *true negatives* (TN) are those cases correctly rejected and *false positives* (FP) are those artifacts incorrectly detected as micro-calcifications. *Specificity* is defined as the probability that the outcome of a breast cancer diagnosis is *negative* given that the patient is healthy according to

$$Specificity = \frac{TN}{TN + FP} = 1 - FPR \quad (11)$$

*Accuracy* is another parameter that becomes a useful tool to assist in the measuring of the performance of the detecting algorithm since it specifies the percentage of breast cancer diagnosis which are correct,

$$Accuracy = \frac{TP + TN}{TP + TN + FP + FN} \quad (12)$$

The *receiver operating characteristic* (ROC) curve compares operating characteristics, TPR vs. FPR by plotting them at different plotting settings. For the case of two classes, a feature vector  $\mathbf{x}$  is classified as Positive or Negative, where  $\mathbf{x}$  is described by a *probability density function*  $f_1(\mathbf{x})$  if it is *Positive* (above a threshold hyper-plane  $\mathcal{T}$ ); otherwise,  $\mathbf{x}$  is described by another *probability density function*  $f_2(\mathbf{x})$ , if it is *Negative* (below a threshold hyper-plane  $\mathcal{T}$ ). Thus, the TPR is given by  $TPR(\mathcal{T}) = \int f_1(\mathbf{x}) d\mathbf{x}$  and the FPR is given by  $FPR(\mathcal{T}) = \int f_2(\mathbf{x}) d\mathbf{x}$ . The ROC plots  $TPR(\mathcal{T})$  versus  $FPR(\mathcal{T})$  as hyper-plane  $\mathcal{T}$  is varied. The *area under the curve* (AUC), given by  $AUC = \int_{-\infty}^{\infty} TPR(FPR) d\mathcal{T}$ , is equal to the probability that a classifier ranks a randomly chosen positive higher than a randomly chosen negative one.

Efficiency is measured in terms of number of lesions and not on number of images. Out of 20 abnormal mammograms and 207 normal mammograms in the MIAS data set, all images were used with 268 micro-calcifications extracted from abnormal mammograms and 268 ROIs, without MC, randomly extracted from normal mammograms. ROIs for MC detection are 21 X 21 pixels. By counting the number of MC candidates, labeled as TP, FP, TN, and FN, the proposed method for MC detection, on the MIAS data set,. The same set of efficiency measurements were carried out with 114 MCs and 114 normal ROIs, extracted from the DDSM data set. ROIs for MC detection are 21 X 21 pixels. The same set of experiments is also applied to MCs and normal candidates from both data sets, MIAS and DDSM. These results are shown in the last five rows of Table 10.

ROC curves, generated by the proposed method, based on the *SVM* classifier and *kNN*, are shown in Figure 20 and Figure 21, respectively. Each Figure shows ROC curves, after applying the corresponding classifier to three different data sets, MIAS, DDSM, and a combination of both. The *AUC* parameter, for each ROC curve, is provided in previous paragraphs and in the first two rows within the last five rows in Table 10.

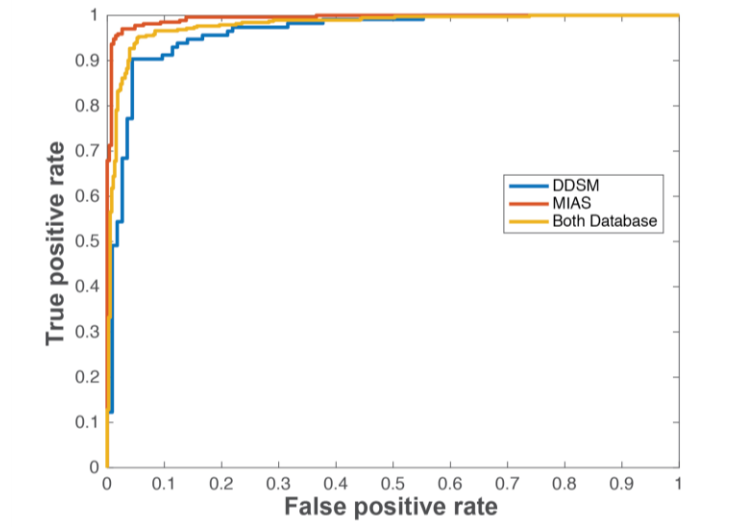


Figure 20. ROC (TPR vs. FPR) obtained by testing the method with the SVM classifier on three different data sets, MIAS (red curve), DDSM (blue curve), and the combination of both data sets (orange curve).

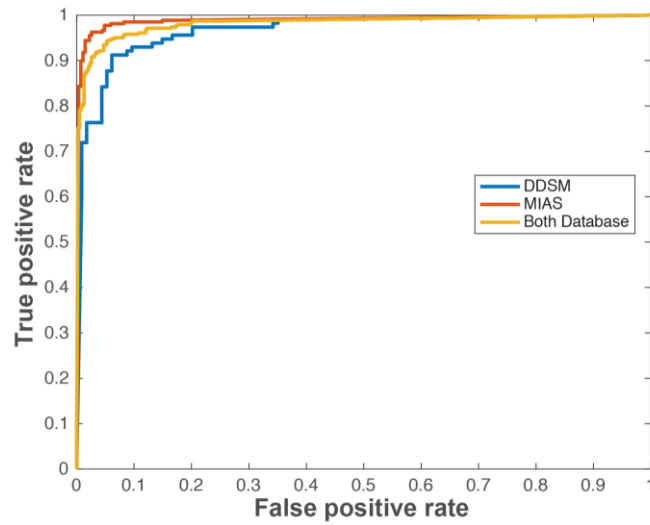


Figure 21. ROC (TPR vs. FPR) obtained by testing the method with the kNN classifier on three different data sets, MIAS (red curve), DDSM (blue curve), and the combination of both data sets (orange curve).

ROC curves, based on the application of the SVM and kNN, are shown in Figure 22 and Figure 23, respectively. Each Figure shows ROC curves, after applying the



corresponding classifier to MIAS mammograms for each breast density: fatty, fatty-glandular, and dense.

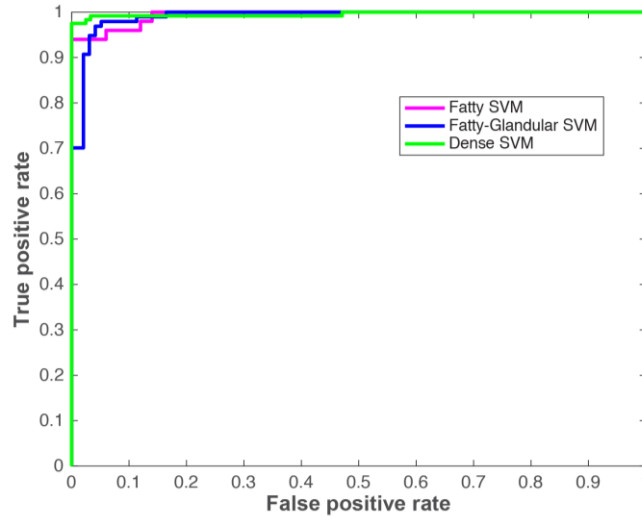


Figure 22. ROC (TPR vs. FPR) obtained by testing the method with the SVM classifier on the MIAS data set for each density group, fatty (purple curve), fatty-glandular (blue curve), and dense (green curve).

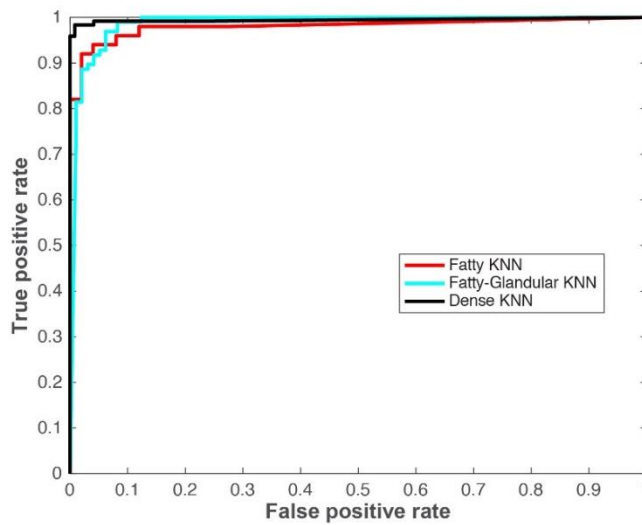


Figure 23. ROC (TPR vs. FPR) obtained by testing the method with the kNN classifier on the MIAS data set for each density group, fatty (red curve), fatty-glandular (green curve), and dense (black curve).

Once a way to segment the MCs has been studied, a model for the detection of MCs was created, while reducing false positives. Table 10 shows the performance of different methods, including the proposed one, in terms of *TPR* or *sensitivity*, *FPR*, *accuracy* and *AUC* where different public data sets are used. The purpose of Table 10 is to show the different data sets, and levels of TPR, FPR, accuracy and AUC, proposed by the scientific community, working on the problem of MC detection. The proposed approach is included among those approaches that use data sets, MIAS and/or DDSM. Some methods do not report some of the performance measures (TPR, FPR, accuracy, AUC). After observing the sixth column of Table 10, it is concluded that our method is the only one which uses all mammograms from each data set. Also, it is the only method which analyzes all the micro-calcifications, extracted from each data set. The method, proposed in [44] , is the second one with the highest TPR (0.9810), at the expense of very high FPR (0.6300), while accuracy and AUC values are not reported. This method is applied to some mammograms from the MIAS data set. Our approach achieves the highest values in terms of TPR, accuracy and AUC, and it also reaches the lowest FPR values.

*Table 10. Performance of different methods for detection of micro-calcifications.*

<b>Ref.</b>	<b>TPR</b>	<b>FPR</b>	<b>Accuracy</b>	<b>AUC</b>	<b>Data set</b>	<b>Number of images</b>
[44]	<b>Both:</b> 0.9810	<b>Both:</b> 0.63 per image			DDSM MIAS	50/322 MIAS im- ages. 140 DDSM im- ages.
[89]	<b>MIAS</b> SVM: 1 <b>DDSM</b> No re- port	<b>MIAS</b> SVM 0.19 <b>DDSM</b> No re- port		<b>MIAS</b> SVM: 0.98 ELM: 0.9941 <b>DDSM</b> SVM: 0.90 ELM 0.9168	DDSM MIAS	26 MIAS ROIs (12 benign, 14 out of 20 malig- nant). 150 DDSM ROIs (82 benign 68 malignant).
[46]			kNN: 0.95 MIAS	kNN: 0.96	DDSM MIAS	Cluster ROIs of 352 X 301.

			kNN: 0.86 DDSM	MIAS kNN: 0.90 DDSM	10 fold	9 out of 20 MIAS ROIs malignant and 11 benign. 14 DDSM ROIs malignant and 11 benign.
[49]	0.97	0.45 per image				Cluster ROIs. 234 ROIs (150 abnormal – 84 normal). MIAS, USCF and DDSM data sets. DDSM images (27 abnormal – 18 normal).
[48]			kNN: 0.95 MIAS kNN: 0.78 DDSM	0.95 MIAS 0.77 DDSM	MIAS	Cluster ROIs of 512 X 512. 20/20 MIAS im- ages. DDSM images with 134 malig- nant – 146 be- nign.
[45]	0.8715		0.9143	0.9036	MIAS	
[41]	0.957		0.959	0.97	MIAS	23 mammograms (7 Glandular, 10 Dense, 6 Fatty) containing micro- calcification clus- ters. 50 mammograms (15 Glandular, 20 Dense, 15 Fatty) without micro- calcifications.
Proposed KNN	0.9386 0.9590 0.9241	0.0702 0.0224 0.0288	0.9664 0.9683 0.9476	0.9742 0.9885 0.9826	DDSM MIAS Both	20/20 MIAS ab- normal images. .
Proposed SVM	0.9211 0.9664 0.9476	0.0526 0.0299 0.0550	0.9342 0.9683 0.9463	0.9656 0.9934 0.9802	DDSM MIAS Both	207/207 MIAS normal images.

Proposed MIAS dense	KNN: 0.9835 SVM: 0.9752	KNN: 0.0165 SVM: 0	KNN: 0.9835 SVM: 0.9876	KNN: 0.9944 SVM: 0.9951		ROIs of 21 X 21 pixels.
Proposed MIAS fatty	KNN: 0.9400 SVM: 0.9200	KNN: 0.04 SVM: 0	KNN: 0.95 SVM: 0.96	KNN: 0.9592 SVM: 0.9928		268 normal can- didates and 268 micro-calcifica- tions on MIAS data set.
Proposed MIAS fatty- glandular	kNN: 0.9897 SVM: 0.9691	KNN: 0.1031 SVM: 0.0309	KNN: 0.9433 SVM: 0.9691	KNN: 0.951 SVM: 0.9930		114 normal can- didates and 114 micro-calcifica- tions on DDSM data set

## *Conclusion and future work*

---

### 4.1 Discussion

The results in Table 9 show that Entropy algorithm has better performance in the three categories, followed by Intermodos method. However, these algorithms did not get close to 100 percent, especially in subtle and cluster category. This was mainly due to the fact that in some images the MCs were 3x3 pixels in size, which could be considered as noise, making it difficult to segment them. It is also always important taking into consideration a fine adjustment for subtle MCs segmentation. Therefore, there is a trade-off between obvious and subtle segmentation when they are together. The Otsu method, despite being the most widely used, showed its clear dependence on bimodal histograms. For this type of images, the value of threshold was not always in the valley of bimodal peaks, as the Otsu method expects. The entropy method works best because it looks for areas where the pixels are similar, that is, less entropy. In most cases the background has a higher entropy level compared to the MCs.

In the case of MCs detection, works of [45], [41], [44], [46], [48]- [49], in Table 10, do not provide enough detail on how it is decided to exclude some data set images from experiments, particularly regarding images with abnormal ROIs. Not including all mammograms from the data set, probably explains the generation of better results than those, obtained by using the whole available set of abnormal images.

Results of the proposed method are better than those from other recent methods, in terms of *sensitivity*, *false positive rate*, *accuracy*, and *area under the ROC curve*; despite the fact that most previous works do not use all the available abnormal images in data sets, and do not explain why some data set images were chosen, and others were not, for their experiments.

This proposed method, that uses an annulus-based micro-calcification model, reflects physical conditions of mammogram into patient condition, which gives

generality. The generality of the model was tested with three different datasets, MIAS, DDSM, and combined.

## 4.2 Conclusion

Important aspects to the solution of this problem are the reduced number of features (just four features), low computational cost, the use of a micro-calcification model based on annular regions which reflects real physical conditions in mammograms from women with MCs, features which are independent of image resolution, outstanding performance results. The proposed method promises a good future because of its simplicity for implementation and the advantage of using a reduced number of features and resources.

After comparing the proposed approach with other recent methods, our approach achieves the best performance in terms of *true positive rate* (TPR) or *sensitivity*, *false positive rate* (FPR), *accuracy*, and *area under the ROC curve*; even though other methods did not include all available abnormal images, from a data set; and the fact that these other works do not specify image selection for experiments. Methods, for MC detection on dense mammograms, show very low performance; however, we give the best performance during MC detection on dense mammograms with 0.9752 for TPR, 0 for FPR, 0.9876 for accuracy, and 0.9951 for AUC.

Table 11, shows the comparison of the best results found in the literature review with the results obtained by the method proposed in this work. The table shows that the area under the curve of the proposed method is the best for both the MIAS database and the DDSM, with both SVM and KNN classifiers. Also, the proportion value of false positives is significantly lower than those reported in the literature.

Table 11. Comparison with our proposed method and the two-best result in literature

Ref.	TPR	FPR	Accu- racy	AUC	Data set	Number of images
[44]	<b>Both:</b> 0.9810	<b>Both:</b> 0.63 per image			DDSM MIAS	50/322 MIAS im- ages.

						140 DDSM im- ages.
[89]	<b>MIAS</b> SVM: 1 <b>DDSM</b> No re- port	<b>MIAS</b> SVM 0.19 <b>DDSM</b> No re- port		<b>MIAS</b> SVM: 0.98 ELM: 0.9941 <b>DDSM</b> SVM: 0.90 ELM 0.9168	DDSM MIAS	26 MIAS ROIs (12 benign, 14 out of 20 malignant). 150 DDSM ROIs (82 benign 68 ma- lignant).
Pro- posed KNN	0.9386 0.9590 0.9241	0.0702 0.0224 0.0288	0.9664 0.9683 0.9476	0.9742 0.9885 0.9826	DDSM MIAS Both	20/20 MIAS ab- normal images. .
Pro- posed SVM	0.9211 0.9664 0.9476	0.0526 0.0299 0.0550	0.9342 0.9683 0.9463	0.9656 0.9934 0.9802	DDSM MIAS Both	207/207 MIAS normal images.
Pro- posed MIAS dense	KNN: 0.9835 SVM: 0.9752	KNN: 0.0165 SVM: 0	KNN: 0.9835 SVM: 0.9876	KNN: 0.9944 SVM: 0.9951		ROIs of 21 X 21 pixels.

As mentioned earlier, it is expected that in the coming years mammography will be completely digital. Therefore, the resolution of the images will increase. Therefore, it is an important factor to be taken into consideration, i.e. the algorithm should be image resolution independent. The algorithm proposed in this work has considered image resolution independence by just modifying the mask for the extraction of the annular regions for a given image resolution.

With respect to the general goal of this work, it was possible to design an algorithm capable of segmenting, detecting and classifying microcalcifications in various types of density, especially for mammograms with dense density areas. Also, the algorithm can be easily adapted for any type of resolution, if the resolution allows the identification of MCs (at least 200 microns per pixel). Also, this algorithm was tested in the two of the most used databases, MIAS, DDSM and a combined set of both, showing

independence of a given database. As demonstrated in the previous chapter, the work presented here is competitive with the most relevant previous works.

### 4.3 Future Work

This dissertation focused on the segmentation and detection of microcalcifications in mammography images. However, it is necessary to implement a preprocessing stage, in which the pectoral area is removed as this can generate false positives as well as prevent the detection of some MCs. This is because the level of intensity that the pectoral has is greater than or equal to the vast majority of MCs present in the mammogram's image. Once the algorithm can be implemented throughout the full image, the MCs could be marked so that the expert can decide on the possible treatment to follow, relieving the expert from having to scan the whole image, thus allowing him/her to analyze many more mammograms in a given time.

Another important aspect that can be done in future work is to use some other databases, both public and private. Likewise, this algorithm can be implemented, as originally proposed, as the first reader in the screening stage. In such a way that the expert can be helped by pointing out the most likely areas to have MCs that she/he should analyze. All this to reduce the workload of the expert and increase his/her productivity.

### 4.4 Contributions

This dissertation contributed to the segmentation of MCs. For this, it was contributed in the definition of MCs according to their surrounding tissue; that is, at the intensity level. So, the MCs were defined as obvious, subtle and cluster. Also, in the segmentation stage it was found that the entropy thresholding method gave better results than the Otsu method, which is the most used. This could be observed by the fact that histograms of MCs are mostly unimodal.

Also, the design of a gray-scale structural model based on annulus was contributed. This model represents the nature of the MCs which makes it independent of breast



density. Also, this model can be easily scaled for any resolution. This was verified when testing this model with two databases with different resolutions.

## References

---

- [1] F. Bray, J. Ferlay, I. Soerjomataram, R. L. Siegel, L. A. Torre, and A. Jemal, “Global cancer statistics 2018: GLOBOCAN estimates of incidence and mortality worldwide for 36 cancers in 185 countries,” *CA. Cancer J. Clin.*, vol. 68, no. 6, pp. 394–424, 2018.
- [2] N. G. Coburn, M. A. Chung, J. Fulton, and B. Cady, “Decreased breast cancer tumor size, stage, and mortality in Rhode Island: An example of a well-screened population,” *Cancer Control*, vol. 11, no. 4, pp. 222–230, Jul. 2004.
- [3] K. R. Cho *et al.*, “Breast Cancer Detection in a Screening Population: Comparison of Digital Mammography, Computer-Aided Detection Applied to Digital Mammography and Breast Ultrasound,” *J. Breast Cancer*, vol. 19, no. 3, p. 316, 2016 [Online]. Available: <http://synapse.koreamed.org/DOIx.php?id=10.4048/jbc.2016.19.3.316>
- [4] U. Fischer *et al.*, “Comparative study in patients with microcalcifications: full-field digital mammography vs screen-film mammography,” *Eur. Radiol.*, vol. 12, no. 11, pp. 2679–2683, 2002.
- [5] American Cancer Society, “Mammogram basics,” *American Cancer Society*, 2014. [Online]. Available: <http://www.cancer.org/healthy/findcancerearly/examandtestdescriptions/mammogramsandotherbreastimagingprocedures/mammograms-and-other-breast-imaging-procedures-what-is-mammogram>
- [6] “Breast Screening - FAQs,” *University of Maryland Medical*, 2014. [Online]. Available: <http://www.umm.edu/programs/breast-center/faqs>. [Accessed: 08-Aug-2017]
- [7] S. Contreras, “How long does it take to get mammogram results,” 2015. [Online]. Available: <https://www.youtube.com/watch?v=RGZIFqATR90>

- [8] S. L. L. Valerie F. Andolina, “Chapter 7 Mammographic Positioning,” in *Mammographic Imaging: A Practical Guide*, pp. 100–159.
- [9] L. Wilkinson, V. Thomas, and N. Sharma, “Microcalcification on mammography: approaches to interpretation and biopsy,” *Br. J. Radiol.*, vol. 90, no. 1069, p. 20160594, Jan. 2017 [Online]. Available: <http://www.birpublications.org/doi/10.1259/bjr.20160594>
- [10] J. Suckling *et al.*, “The Mammographic Image Analysis Society Digital Mammogram Database,” *Expert. Medica, Int. Congr. Ser.*, vol. 1069, no. JANUARY 1994, pp. 375–378, 1994 [Online]. Available: [http://www.researchgate.net/publication/247927550\\_The\\_Mammographic\\_Image\\_Analysis\\_Society\\_Digital\\_Mammogram\\_Database](http://www.researchgate.net/publication/247927550_The_Mammographic_Image_Analysis_Society_Digital_Mammogram_Database)”Exerpta\_Medica
- [11] M. Heath, K. Bowyer, D. Kopans, R. Moore, and P. Kegelmeyer, “The digital database for screening mammography,” *Proc. Fifth Int. Work. Digit. Mammogr.*, pp. 212–218, 2001 [Online]. Available: [http://www.nd.edu/~kwb/HeathEtAlIWDM\\_2000.pdf%5Cnpapers2://publication/uuid/37C3C3F3-5994-4145-AB4B-5B1CC5381282](http://www.nd.edu/~kwb/HeathEtAlIWDM_2000.pdf%5Cnpapers2://publication/uuid/37C3C3F3-5994-4145-AB4B-5B1CC5381282)
- [12] S. P. Weinstein, “Screening Mammography,” in *Radiology Secrets Plus*, Elsevier, 2011, pp. 29–33 [Online]. Available: <https://linkinghub.elsevier.com/retrieve/pii/B9780323067942000055>
- [13] I. C. Moreira, I. Amaral, I. Domingues, A. Cardoso, M. J. Cardoso, and J. S. Cardoso, “INbreast: Toward a Full-field Digital Mammographic Database.,” *Acad. Radiol.*, vol. 19, no. 2, pp. 236–248, 2012.
- [14] G. N. Hortobagyi *et al.*, “Breast,” in *AJCC Cancer Staging Manual*, vol. 57, Cham: Springer International Publishing, 2017, pp. 589–636 [Online]. Available: [https://cancerstaging.org/references-tools/deskreferences/Documents/AJCC Breast Cancer Staging System.pdf](https://cancerstaging.org/references-tools/deskreferences/Documents/AJCC_Breast_Cancer_Staging_System.pdf)
- [15] Jordan breastcancer program, “Breast Cancer Staging | Jordan Breast Cancer

- Program.” [Online]. Available:  
<http://www.jbcp.jo/understandingbreastcancer/33>
- [16] The American Cancer Society medical and editorial content team, “Types of Breast Cancer,” *American Cancer Society*, 2016. [Online]. Available:  
<https://www.cancer.org/cancer/breast-cancer/understanding-a-breast-cancer-diagnosis/types-of-breast-cancer.html>. [Accessed: 08-Aug-2017]
- [17] Breastcancer.org, “Diagnosis of DCIS,” 2015. [Online]. Available:  
<http://www.breastcancer.org/symptoms/types/dcis/diagnosis>. [Accessed: 18-Dec-2017]
- [18] C. F. Cowell *et al.*, “Progression from ductal carcinoma in situ to invasive breast cancer: Revisited,” *Mol. Oncol.*, vol. 7, no. 5, pp. 859–869, 2013 [Online]. Available: <http://dx.doi.org/10.1016/j.molonc.2013.07.005>
- [19] P. Henrot, A. Leroux, C. Barlier, and P. Génin, “Breast microcalcifications: The lesions in anatomical pathology,” *Diagn. Interv. Imaging*, vol. 95, no. 2, pp. 141–152, Feb. 2014 [Online]. Available:  
<https://linkinghub.elsevier.com/retrieve/pii/S2211568413003884>
- [20] M. Mustra, M. Grgic, and R. M. Rangayyan, “Review of recent advances in segmentation of the breast boundary and the pectoral muscle in mammograms,” *Med. Biol. Eng. Comput.*, vol. 54, no. 7, pp. 1003–1024, 2016.
- [21] H. Al-Ghaib, “Temporal Mammogram Segmentation for improving early breast cancer detection,” University of Alabama, 2015 [Online]. Available:  
<https://search.proquest.com/openview/ef55a1f73b13f1b6998c9779083725bd/1?pq-origsite=gscholar&cbl=18750&diss=y>
- [22] M. A. Wirth and A. Stapinski, “Segmentation of the breast region in mammograms using active contours,” in *Proc. SPIE 5150, Visual Communications and Image Processing 2003*, 2003, pp. 1995–2006 [Online]. Available:

<http://proceedings.spiedigitallibrary.org/proceeding.aspx?articleid=768088>

- [23] M. A. Wirth, J. Lyon, and D. Nikitenko, "A fuzzy approach to segmenting the breast region in mammograms," *IEEE Annu. Meet. Fuzzy Information, 2004. Process. NAFIPS '04.*, pp. 474-479 Vol.1, 2004 [Online]. Available: <http://ieeexplore.ieee.org/document/1336329/>
- [24] A. Touil and K. Kalti, "Iterative fuzzy segmentation for an accurate delimitation of the breast region," *Comput. Methods Programs Biomed.*, vol. 132, pp. 137–147, 2016 [Online]. Available: <http://dx.doi.org/10.1016/j.cmpb.2016.04.020>
- [25] Z. Yang *et al.*, "A new method of micro-calcifications detection in digitized mammograms based on improved simplified PCNN," *Neurocomputing*, vol. 218, no. 222, pp. 79–90, Dec. 2016 [Online]. Available: <http://dx.doi.org/10.1016/j.cmpb.2016.02.019>
- [26] V. B. Bora, A. G. Kothari, and A. G. Keskar, "Robust Automatic Pectoral Muscle Segmentation from Mammograms Using Texture Gradient and Euclidean Distance Regression," *J. Digit. Imaging*, vol. 29, no. 1, pp. 115–125, 2016.
- [27] W. B. Yoon, J. E. Oh, E. Y. Chae, H. H. Kim, S. Y. Lee, and K. G. Kim, "Automatic Detection of Pectoral Muscle Region for Computer-Aided Diagnosis Using MIAS Mammograms," *Biomed Res. Int.*, vol. 2016, pp. 1–6, 2016 [Online]. Available: <https://www.hindawi.com/journals/bmri/2016/5967580/>
- [28] Xu Weidong and Xia Shunren, "A model based algorithm to segment the pectoral muscle in mammograms," in *International Conference on Neural Networks and Signal Processing, 2003. Proceedings of the 2003*, 2003, pp. 1163-1169 Vol.2 [Online]. Available: <http://ieeexplore.ieee.org/document/1281076/>
- [29] W. Xu, H. Li, and W. Liu, "A novel pectoral muscle segmentation algorithm

- based on polyline fitting and elastic thread approaching,” *2007 1st Int. Conf. Bioinforma. Biomed. Eng. ICBBE*, pp. 837–840, 2007.
- [30] R. J. Ferrari, R. M. Rangayyan, J. E. L. Desautels, R. A. Borges, and A. F. Frère, “Automatic Identification of the Pectoral Muscle in Mammograms,” *IEEE Trans. Med. Imaging*, vol. 23, no. 2, pp. 232–245, 2004.
  - [31] W. Peng, R. V. Mayorga, and E. M. A. Hussein, “An automated confirmatory system for analysis of mammograms,” *Comput. Methods Programs Biomed.*, vol. 125, pp. 134–144, 2016 [Online]. Available: <http://dx.doi.org/10.1016/j.cmpb.2015.09.019>
  - [32] H. AL-GHAIB, “Temporal Mammogram Segmentation for improving early breast cancer detection,” University of Alabama, 2015.
  - [33] A. Rojas Domínguez and A. K. Nandi, “Detection of masses in mammograms via statistically based enhancement, multilevel-thresholding segmentation, and region selection,” *Comput. Med. Imaging Graph.*, vol. 32, no. 4, pp. 304–315, 2008.
  - [34] T. Kooi and N. Karssemeijer, “Deep learning of symmetrical discrepancies for computer-aided detection of mammographic masses,” in *SPIE 10134, Medical Imaging 2017: Computer-Aided Diagnosis*, 2017, vol. 10134, p. 101341J [Online]. Available: <http://proceedings.spiedigitallibrary.org/proceeding.aspx?doi=10.1117/12.2254586>
  - [35] A. Vadivel and B. Surendiran, “A fuzzy rule-based approach for characterization of mammogram masses into BI-RADS shape categories,” *Comput. Biol. Med.*, vol. 43, no. 4, pp. 259–267, 2013 [Online]. Available: <http://dx.doi.org/10.1016/j.compbimed.2013.01.004>
  - [36] S. C. Ling, A. A. Abdullah, and W. K. W. Ahmad, “Design of an Automated Breast Cancer Masses Detection in Mammogram Using Cellular Neural

- Network (CNN) Algorithm,” *Adv. Sci. Lett.*, vol. 20, no. 1, pp. 254–258, Jan. 2014 [Online]. Available: <http://www.ingentaconnect.com/content/10.1166/asl.2014.5307>
- [37] J. Dheeba and G. Wiselin Jiji, “Detection of Microcalcification Clusters in Mammograms using Neural Network,” *Int. J. Adv. Sci. Technol.*, vol. 19, no. 1, pp. 13–22, 2010.
- [38] P. S. Vikhe and V. R. Thool, “Mass Detection in Mammographic Images Using Wavelet Processing and Adaptive Threshold Technique,” *J. Med. Syst.*, vol. 40, no. 4, pp. 1–16, 2016.
- [39] Z. Lu, G. Carneiro, N. Dhungel, and A. P. Bradley, “Automated Detection of Individual Micro-calcifications from Mammograms using a Multi-stage Cascade Approach,” *CoRR*, vol. abs/1610.0, Oct. 2016 [Online]. Available: <http://arxiv.org/abs/1610.02251>
- [40] M. S. Islam, “Microcalcifications detection using image and signal processing techniques for early detection of breast cancer,” University of North Dakota, 2016 [Online]. Available: <https://commons.und.edu/theses/2029/>
- [41] Y. Y. Guo *et al.*, “A new method of detecting micro-calcification clusters in mammograms using contourlet transform and non-linking simplified PCNN,” *Comput. Methods Programs Biomed.*, vol. 130, no. 222, pp. 31–45, 2016 [Online]. Available: <http://dx.doi.org/10.1016/j.cmpb.2016.02.019>
- [42] L. Vivona, D. Cascio, F. Fauci, and G. Raso, “Fuzzy technique for microcalcifications clustering in digital mammograms,” *BMC Med. Imaging*, vol. 14, no. 1, p. 23, 2014 [Online]. Available: <http://www.ncbi.nlm.nih.gov/pubmed/24961885>
- [43] H. Mohamed, M. S. Mabrouk, and A. Sharawy, “Computer aided detection system for micro calcifications in digital mammograms,” *Comput. Methods Programs Biomed.*, vol. 116, no. 3, pp. 226–235, 2014 [Online]. Available:

<http://dx.doi.org/10.1016/j.cmpb.2014.04.010>

- [44] A. a. AbuBaker, “Automatic Microcalcification Detection Using Wavelet Transform,” *Int. J. Comput. Theory Eng.*, vol. 7, no. 1, pp. 40–45, 2014 [Online]. Available:  
<http://www.ijcte.org/index.php?m=content&c=index&a=show&catid=61&id=1110>
- [45] F. Pak, H. R. Kanan, and A. Alikhassi, “Breast cancer detection and classification in digital mammography based on Non-Subsampled Contourlet Transform (NSCT) and Super Resolution,” *Comput. Methods Programs Biomed.*, vol. 122, no. 2, pp. 89–107, 2015 [Online]. Available:  
<http://dx.doi.org/10.1016/j.cmpb.2015.06.009>
- [46] Z. Chen, H. Strange, A. Oliver, E. R. E. Denton, C. Boggis, and R. Zwiggelaar, “Topological Modeling and Classification of Mammographic Microcalcification Clusters,” *IEEE Trans. Biomed. Eng.*, vol. 62, no. 4, pp. 1203–1214, 2015.
- [47] M. A. Duarte, A. V. Alvarenga, C. M. Azevedo, M. J. G. Calas, A. F. C. Infantsi, and W. C. A. Pereira, “Evaluating geodesic active contours in microcalcifications segmentation on mammograms,” *Comput. Methods Programs Biomed.*, vol. 122, no. 3, pp. 304–315, 2015 [Online]. Available:  
<http://dx.doi.org/10.1016/j.cmpb.2015.08.016>
- [48] O. Ashiru and R. Zwiggelaar, “Classification of mammographic microcalcification clusters using a combination of topological and location modelling,” in *2016 Sixth International Conference on Image Processing Theory, Tools and Applications (IPTA)*, 2016, pp. 1–6 [Online]. Available:  
<http://ieeexplore.ieee.org/document/7820986/>
- [49] M. Muthuvel, B. Thangaraju, and G. Chinnasamy, “Microcalcification cluster detection using multiscale products based Hessian matrix via the Tsallis thresholding scheme,” *Pattern Recognit. Lett.*, 2017 [Online]. Available:



<http://linkinghub.elsevier.com/retrieve/pii/S0167865517301447>

- [50] M. A. Duarte, A. V. Alvarenga, C. M. Azevedo, M. J. G. Calas, A. F. C. Infantosi, and W. C. A. Pereira, “Evaluating geodesic active contours in microcalcifications segmentation on mammograms,” *Comput. Methods Programs Biomed.*, vol. 122, no. 3, pp. 304–315, 2015 [Online]. Available: <http://dx.doi.org/10.1016/j.cmpb.2015.08.016>
- [51] A. J. Bekker, M. Shalhon, H. Greenspan, and J. Goldberger, “Multi-view probabilistic classification of breast microcalcifications,” *IEEE Trans. Med. Imaging*, vol. 35, no. 2, pp. 645–6536, 2016.
- [52] S. Y. Shin *et al.*, “A Novel Cascade Classifier for Automatic Microcalcification Detection,” *PLoS One*, vol. 10, no. 12, p. e0143725, Dec. 2015 [Online]. Available: <http://dx.plos.org/10.1371/journal.pone.0143725>. [Accessed: 09-Jan-2017]
- [53] P. Cunningham and S. J. Delany, “K -Nearest Neighbour Classifiers,” *Mult. Classif. Syst.*, no. May, pp. 1–17, 2007.
- [54] R. Berwick and V. Idiot, “An Idiot ’ s guide to Support vector machines ( SVMs ) SVMs : A New Generation of Learning Algorithms Key Ideas,” pp. 1–28, 1990.
- [55] Instituto Nacional de Estadística y Geografía, “Estadísticas a Propósito Del... Día Mundial De La Lucha Contra El Cáncer De Mama,” p. 14, 2105 [Online]. Available: <http://www.inegi.org.mx/saladeprensa/aproposito/2015/mama0.pdf>
- [56] P. Autier, D. Ait Ouakrim, and D. A. Ouakrim, “Determinants of the number of mammography units in 31 countries with significant mammography screening.,” *Br. J. Cancer*, vol. 99, no. 7, pp. 1185–90, 2008 [Online]. Available: <http://www.ncbi.nlm.nih.gov/pubmed/18781176> <http://www.pubmedcentral.nih.gov/articlerender.fcgi?artid=PMC2567070>
- [57] R. Rodríguez, “Una amenaza que nos moviliza,” *El universal*, 2012. [Online].

Available: <http://archivo.eluniversal.com.mx/primer/40571.html>

- [58] D. Macro, “México - Piramide de población 2018.” [Online]. Available: <https://datosmacro.expansion.com/demografia/estructura-poblacion/mexico>
- [59] S. de Salud., “Cáncer de Mama. Mastografía,” 2015. [Online]. Available: <https://www.gob.mx/salud/acciones-y-programas/cancer-de-mama-mastografia>
- [60] E. Kreit *et al.*, “Biological versus electronic adaptive coloration: how can one inform the other?,” *J. R. Soc. Interface*, vol. 10, no. 78, pp. 20120601-, 2012 [Online]. Available: <http://rsif.royalsocietypublishing.org/content/10/78/20120601.abstract>
- [61] N. C. Institute, “Mammograms,” 2016. [Online]. Available: <https://www.cancer.gov/types/breast/mammograms-fact-sheet#q1>. [Accessed: 08-Aug-2017]
- [62] M. Noble, W. Bruening, S. Uhl, and K. Schoelles, “Computer-aided detection mammography for breast cancer screening: Systematic review and meta-analysis,” *Arch. Gynecol. Obstet.*, vol. 279, no. 6, pp. 881–890, 2009.
- [63] E. L. Henriksen, J. F. Carlsen, I. M. M. Vejborg, M. B. Nielsen, and C. A. Lauridsen, “The efficacy of using computer-aided detection (CAD) for detection of breast cancer in mammography screening: a systematic review,” *Acta radiol.*, vol. 60, no. 1, pp. 13–18, Jan. 2019 [Online]. Available: <http://journals.sagepub.com/doi/10.1177/0284185118770917>
- [64] P. Hannah, “The False Negative Rate of Digital Mammography at an American Academic Medical Center,” *Harvard Medical School Teaching Hospital*. 2012 [Online]. Available: <http://www.springerlink.com/index/A1PMR5183M70325K.pdf>
- [65] K. Clark *et al.*, “The Cancer Imaging Archive (TCIA): Maintaining and Operating a Public Information Repository,” *J. Digit. Imaging*, vol. 26, no. 6, pp. 1045–1057, Dec. 2013 [Online]. Available:

<http://link.springer.com/10.1007/s10278-013-9622-7>

- [66] R. S. Lee, F. Gimenez, A. Hoogi, K. K. Miyake, M. Gorovoy, and D. L. Rubin, “A curated mammography data set for use in computer-aided detection and diagnosis research,” *Sci. Data*, vol. 4, no. 1, p. 170177, Dec. 2017 [Online]. Available: <http://www.nature.com/articles/sdata2017177>
- [67] M. Ciecholewski, “Microcalcification Segmentation from Mammograms: A Morphological Approach,” *J. Digit. Imaging*, vol. 30, no. 2, pp. 172–184, 2017.
- [68] B. Kurt, V. V. Nabiyevev, and K. Turhan, “A Novel Algorithm for Segmentation of Suspicious Microcalcification Regions on Mammograms,” in *Lecture Notes in Computer Science (including subseries Lecture Notes in Artificial Intelligence and Lecture Notes in Bioinformatics)*, vol. 9043, 2015, pp. 222–230 [Online]. Available: [http://link.springer.com/10.1007/978-3-319-16483-0\\_23](http://link.springer.com/10.1007/978-3-319-16483-0_23)
- [69] V. D. Nguyen, T. Van Nguyen, T. D. Nguyen, D. T. Nguyen, and H. Van Hoang, “Detect abnormalities in mammograms by local contrast thresholding and rule-based classification,” *ICCE 2010 - 3rd Int. Conf. Commun. Electron.*, pp. 207–210, 2010.
- [70] F. J. López-Aligué, A. Poveda-Pierola, I. Acevedo-Sotoca, and F. García-Urra, “Detection of microcalcifications in digital mammograms,” *Annu. Int. Conf. IEEE Eng. Med. Biol. - Proc.*, pp. 3906–3909, 2007.
- [71] M. Melloul and L. Joskowicz, “Segmentation of microcalcification in X-ray mammograms using entropy thresholding,” *CARS 2002 Comput. Assist. Radiol. Surg.*, pp. 671–676, 2002.
- [72] R. M. Nishikawa, M. L. Giger, K. Doi, C. J. Vyborny, and R. A. Schmidt, “Computer-aided detection of clustered microcalcifications on digital mammograms,” *Med. Biol. Eng. Comput.*, vol. 33, no. 2, pp. 174–178, Mar. 1995 [Online]. Available: <http://link.springer.com/10.1007/BF02523037>
- [73] C. Trull and L. J. Schiller, “Proposed Rules,” *Federal Register*, vol. 84, no. 180.

pp. 11669–11686, 2019.

- [74] U. Hospitals, “Breast Density in U.S.” 2015.
- [75] H. Shen, “A novel image enhancement method for mammogram images,” Western Carolina University, 2013.
- [76] M. Sezgin and B. Sankur, “Survey over image thresholding techniques and quantitative performance evaluation,” *J. Electron. Imaging*, vol. 13, no. 1, p. 220, 2004.
- [77] C. A. Glasbey, “An Analysis of Histogram-Based Thresholding Algorithms,” *CVGIP: Graphical Models and Image Processing*, vol. 55, no. 6. pp. 532–537, 1993 [Online]. Available: <http://www.sciencedirect.com/science/article/pii/S1049965283710400>
- [78] J. M. S. Prewitt and M. L. Mendelsohn, “The analysis of cell images,” *Ann. N. Y. Acad. Sci.*, vol. 128, no. 3, pp. 1035–1053, 1966 [Online]. Available: <http://doi.wiley.com/10.1111/j.1749-6632.1965.tb11715.x>
- [79] J. Kittler and J. Illingworth, “Minimum error thresholding,” *Pattern Recognit.*, vol. 19, no. 1, pp. 41–47, 1986.
- [80] J. N. Kapur, P. K. Sahoo, and A. K. C. Wong, “A New Method for Gray-Level Picture Thresholding Using the Entropy of the Histogram,” *Computer Vision Graphics and Image Processing*, vol. 29. pp. 273–285, 1985.
- [81] N. Otsu, “A threshold selection method from gray-level histograms,” *IEEE Trans. Syst. Man. Cybern.*, vol. 9, no. 1, pp. 62–66, 1979 [Online]. Available: <http://ieeexplore.ieee.org/lpdocs/epic03/wrapper.htm?arnumber=4310076>
- [82] J. Hernandez-Capistran and J. F. Martinez-Carballido, “Thresholding methods review for microcalcifications segmentation on mammography images in obvious, subtle, and cluster categories,” in *2016 13th International Conference on Electrical Engineering, Computing Science and Automatic Control, CCE*

2016, 2016.

- [83] R. M. Haralick, S. R. Sternberg, and X. Zhuang, "Image Analysis Using Mathematical Morphology," *IEEE Trans. Pattern Anal. Mach. Intell.*, vol. 9, no. 4, pp. 532–550, 1987.
- [84] P. Soille, "Morphological gradients," *J. Electron. Imaging*, vol. 2, no. 4, p. 326, Oct. 1993 [Online]. Available: <http://electronicimaging.spiedigitallibrary.org/article.aspx?doi=10.1117/12.159642>
- [85] J. Anitha, J. Dinesh Peter, and S. Immanuel Alex Pandian, "A dual stage adaptive thresholding (DuSAT) for automatic mass detection in mammograms," *Comput. Methods Programs Biomed.*, vol. 138, pp. 93–104, 2017 [Online]. Available: <http://dx.doi.org/10.1016/j.cmpb.2016.10.026>
- [86] D. C. Pereira, R. P. Ramos, and M. Z. do Nascimento, "Segmentation and detection of breast cancer in mammograms combining wavelet analysis and genetic algorithm," *Comput. Methods Programs Biomed.*, vol. 114, no. 1, pp. 88–101, 2014 [Online]. Available: <http://dx.doi.org/10.1016/j.cmpb.2014.01.014>
- [87] A. Qasem *et al.*, "Breast cancer mass localization based on machine learning," *2014 IEEE 10th Int. Colloq. Signal Process. its Appl.*, pp. 31–36, 2014 [Online]. Available: <http://ieeexplore.ieee.org/lpdocs/epic03/wrapper.htm?arnumber=6805715>
- [88] J. Hernández-Capistrán, J. F. Martínez-Carballido, and R. Rosas-Romero, "False Positive Reduction by an Annular Model as a Set of Few Features for Microcalcification Detection to Assist Early Diagnosis of Breast Cancer," *J. Med. Syst.*, vol. 42, no. 8, p. 134, 2018 [Online]. Available: <https://doi.org/10.1007/s10916-018-0989-3>
- [89] K. Hu, W. Yang, and X. Gao, "Microcalcification diagnosis in digital

mammography using extreme learning machine based on hidden Markov tree model of dual-tree complex wavelet transform,” *Expert Syst. Appl.*, vol. 86, pp. 135–144, Nov. 2017 [Online]. Available: <http://linkinghub.elsevier.com/retrieve/pii/S0957417417303901>

Download at: <https://doi.org/10.1109/ICEEE.2016.7751192>

2016 13th International Conference on Electrical Engineering, Computing  
Science and Automatic Control (CCE), Mexico, City, Mexico

## Thresholding Methods Review for Microcalcifications Segmentation on Mammography Images in Obvious, Subtle, and Cluster Categories

Jonathan Hernández-Capistrán, Jorge F. Martínez-Carballido

Electronics Department  
National Institute of Astrophysics, Optics, and Electronics  
Tonantzintla, Puebla/México  
{capistran, jmc}@inaoep.mx

**Abstract**— Microcalcifications are the earliest sign of breast carcinoma. Their typical size is about 1 mm, which is why it is difficult to detect for an expert. Therefore, a tool that eases their visualization becomes relevant. Segmentation gives the candidate areas that could contain microcalcifications. A preprocessing step can improve segmentation performance but the algorithm becomes database dependent. This paper compares four commonly used thresholding techniques to segment mammography images having sections divided in three groups: obvious, subtle and clusters; due to their microcalcification contents. The purpose of this paper is to show what technique has a better performance in special relation with mammography images. Best performers are Entropy (68.8%), and Intermodes (50.9%), but further research is needed to improve performance on subtle and cluster microcalcifications considering non-bimodal histograms.

**Keywords**—Microcalcification, breast cancer, mammography, thresholding, CAD.

### I. INTRODUCTION

Worldwide in women, of all cancer types, breast cancer is the one with highest frequency and with high mortality risk [1]. However, there is not absolute certainty why every year one million cases of breast cancer are detected and 400 000 women die from this cause. It is estimated that in 2012 1.7 million new cases and 521 900 deaths from this cause were detected worldwide [2]. Due to the increase in population and the medical infrastructure, countries with medium and less developed are most affected. In addition, 80% of cancer cases detected in low-income countries is at a stage where a cure is impossible and palliation is the only possible treatment. For breast cancer in high-resource countries, the fatality rate is 23.9, while for low-income countries is 56.3[3]. Early detection of cancer does the treatment easier, reducing risks and the percentage of mortality up to 25% [1]. For early detection, general practice, recommends taking a mammogram for group at risk (mainly postmenopausal) every two years. A microcalcification to reach 1 mm takes about 5 years, and another 3 to 4 years to measure 2 cm; the latter is enough to be detected by palpation [4]. Microcalcifications are the earliest sign of breast cancers and their detection is fundamental for breast cancer control [5]. Therefore, the adoption of computer-

aided diagnosis (CAD for short) is an increasingly necessary tool. A CAD system is a set of semiautomatic or automatic tools developed to assist radiologists in the detection and/or classification of abnormalities in mammograms. [6]. The procedure performed for CAD can be summarized in four essential stages, pre-processing, segmentation, characterization and classification [1]. Although the algorithms that use a pre-processing stage has better performance compared to those, which do not use this stage; however, they are more dependent on the database used. Such that, their performance decrease drastically if the database changes. One of the crucial steps for detecting microcalcifications is the segmentation stage [7], [8]. Thresholding as the most used and simple [9], [10], [11]. This paper compares four important thresholding techniques to show their performances on three microcalcification categories.

### II. THRESHOLDING ALGORITHMS

From a literature review [12] [13] the most commonly used thresholding algorithms are proposed by Prewitt-Mendelsohn (most commonly known as Intermodes) [14], Kittler-Illingworth [15], Kapur et al (most commonly known as Entropy) [16] and Otsu [17]. We begin explaining each one using Fig. 1 as a test image. This image is 76 x 76 pixels; this size was chosen supposing 4x4 windows of 19 x 19 pixels. A window of 19 x 19 is used given that the expected maximum size of a microcalcification is 11 x 11 pixels so it could have about 25 lesions per test image, for INbreast database [18]. The 19x19 considers that some part of the background is necessary to identify the lesions.

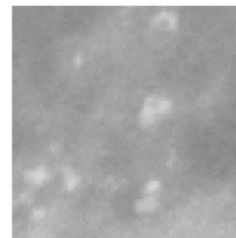


Fig. 1 Image used to analyse different type of algorithms, its size is 76 X 76.

Download at: <https://doi.org/10.1007/s10916-018-0989-3>

Journal of Medical Systems (2018) 42:134  
<https://doi.org/10.1007/s10916-018-0989-3>

IMAGE & SIGNAL PROCESSING



## False Positive Reduction by an Annular Model as a Set of Few Features for Microcalcification Detection to Assist Early Diagnosis of Breast Cancer

Jonathan Hernández-Capistrán<sup>1</sup> · Jorge F. Martínez-Carballido<sup>1</sup> · Roberto Rosas-Romero<sup>2</sup>

Received: 25 March 2018 / Accepted: 7 June 2018  
© Springer Science+Business Media, LLC, part of Springer Nature 2018

### Abstract

Early automatic breast cancer detection from mammograms is based on the extraction of lesions, known as *microcalcifications* (MCs). This paper proposes a new and simple system for *microcalcification detection* to assist in early breast cancer detection. This work uses the two most recognized public mammogram databases, MIAS and DDSM. We are introducing a MC detection method based on (1) Beucher gradient for detection of *regions of interest* (ROIs), (2) an annulus model for extraction of few and effective features from candidates to MCs, and (3) one classification stage with two different classifiers, *k Nearest Neighbor* (KNN) and *Support Vector Machine* (SVM). For dense mammograms in the MIAS database, the performance metrics achieved are *sensitivity* of 0.9835, *false alarm rate* of 0.0083, *accuracy* of 0.9835, and *area under the ROC curve* of 0.9980 with a KNN classifier. The proposed MC detection method, based on a KNN classifier, achieves, a *sensitivity*, *false positive rate*, *accuracy* and *area under the ROC curve* of 0.9813, 0.0224, 0.9795 and 0.9974 for the MIAS database; and 0.9035, 0.0439, 0.9298 and 0.9759 for the DDSM database. By slightly reducing the true positive rate the method achieves *three instances with false positive rate of 0*: 2 on fatty mammograms with KNN and SVM, and one on dense with SVM. The proposed method gives better results than those from state of the art literature, when the mammograms are classified in *fatty*, *fatty-glandular*, and *dense*.

**Keywords** Digital mamograms, microcalcifications · K-nearest neighbors · Support vector machine · Morphologic image processing · Feature extraction

### Introduction

Breast cancer is the number one cause of deaths in women and it corresponds to approximately 15% of all cancer deaths

among women. Worldwide, 570,000 women died of breast cancer in 2015 [1].

Numerous experiments have established that an early detection of cancer eases the treatment, reducing risks, as well as the mortality percentage in 25% [2]. For early detection, *mammography* is an imaging tool with high sensitivity and it is the most recommended by the guidelines of the World Health Organization [3, 4].

A mammogram is the best diagnostic tool to find a cluster of microcalcifications (MCs) in a glandular duct. MCs appear as white specks [5], and they are early signs of breast cancer. Microcalcification lesions are difficult to detect by human vision since microcalcification size is between 0.5 to 2 mm. For this reason, the *false positive rate* of a radiologist is reported at 15% [6] and the *false negative rate* at 20% [7].

This work proposes an algorithm, which detects microcalcifications on mammograms based on morphologic processing, learning machines and a very small set of features. These arguments encourage the implementation of autonomous diagnostic tools to detect early risks of breast cancer by finding

This article is part of the Topical Collection on *Image & Signal Processing*

✉ Jonathan Hernández-Capistrán  
jhcapistran@gmail.com

Jorge F. Martínez-Carballido  
jmc@inaoep.mx

Roberto Rosas-Romero  
roberto.rosas@udlap.mx

<sup>1</sup> Instituto Nacional de Astrofísica, Óptica y Electrónica, Luis Enrique Erro # 1, Santa María Tonantzintla, 72840 Puebla, Pue, Mexico

<sup>2</sup> Universidad de las Américas-Puebla, San Andrés, Cholula, Puebla, Mexico